A robust numerical method for approximating solutions of a model of two-phase flows and its properties

Mai Duc Thanh, Dietmar Kröner, and Christophe Chalons

Department of Mathematics, International University, Quarter 6, Linh Trung Ward, Thu Duc District, Ho Chi Minh City, Vietnam. E-mail address: mdthanh@hcmiu.edu.vn.

Institute of Applied Mathematics, University of Freiburg, Hermann-Herder Str. 10, 79104 Freiburg, Germany.E-mail address: Dietmar.Kroener@mathematik.uni-freiburg.de.

Université Paris 7 and Laboratoire Jacques-Louis Lions, U.M.R. 7598, Boîte courrier 187, 75252 Paris Cedex 05, France. E-mail address: chalons@math.jussieu.fr.

Abstract

The objective of the present paper is to extend our recent works and see what happen on numerical approximations to a more complicated model of two-phase flows, which has applications in the modeling of deflagration-to-detonation transition in granular materials. First, we transform the system into an equivalent one which can be regarded as a composition of three subsystems. Then, depending on the characterization of each subsystem, we propose a convenient numerical treatment of the subsystem separately. Precisely, in the first subsystem of the governing equations in the gas phase, stationary waves are used to absorb the nonconservative terms into an underlying numerical scheme. In the second subsystem of conservation laws of the mixture we can take a suitable scheme for conservation laws. For the third subsystem of the compaction dynamics equation, the fact that the velocities remain constant across solid contacts suggests us to employ the technique of Engquist-Osher's scheme. Then, we prove that our method possesses some interesting properties: it preserves the positivity of the volume fractions in both phases, and in the gas phase, our scheme is capable of capturing equilibrium states, preserves the positivity of the density, and satisfies the numerical minimum entropy principle. Numerical tests show that our scheme can provide reasonable approximations for data the supersonic regions, but the results are not satisfactory in the subsonic region. However, the scheme is numerically stable and robust.

Keywords: Two-phase flow, conservation law, source term, numerical approximation, well-balanced scheme, positivity of density, minimum entropy principle.

1. Introduction

We consider numerical approximations of a model of two-phase flows which is used for the modeling of deflagration-to-detonation transition in porous energetic materials. Precisely, the model consists of six governing equations representing the balance of mass,

momentum and energy in each phase, namely,

$$\begin{array}{l}
\partial_t(\alpha_g\rho_g) + \partial_x(\alpha_g\rho_g u_g) = 0,\\
\partial_t(\alpha_g\rho_g u_g) + \partial_x(\alpha_g(\rho_g u_g^2 + p_g)) = p_g\partial_x\alpha_g,\\
\partial_t(\alpha_g\rho_g e_g) + \partial_x(\alpha_g u_g(\rho_g e_g + p_g)) = p_g u_s\partial_x\alpha_g,\\
\partial_t(\alpha_s\rho_s) + \partial_x(\alpha_s\rho_s u_s) = 0,\\
\partial_t(\alpha_s\rho_s u_s) + \partial_x(\alpha_s(\rho_s u_s^2 + p_s)) = p_g\partial_x\alpha_s,\\
\partial_t(\alpha_s\rho_s e_s) + \partial_x(\alpha_s u_s(\rho_s e_s + p_s)) = p_g u_s\partial_x\alpha_s, \quad x \in \boldsymbol{R}, t > 0,
\end{array} \tag{1.1}$$

together with the compaction dynamics equation

$$\partial_t\alpha_g + u_s\partial_x\alpha_g = 0, \quad x \in \boldsymbol{R}, t > 0, \tag{1.2}$$

see [6, 11]. Throughout, we use the subscripts g and s to indicate the quantities in the gas phase and in the solid phase, respectively. The notations $\alpha_k, \rho_k, u_k, p_k, \varepsilon_k, S_k, T_k, e_k = \varepsilon_k + u_k^2/2, k = g, s$, respectively, stand for the volume fraction, density, velocity, pressure, internal energy, specific entropy, temperature, and the total energy in the k-phase, $k = g, s$, respectively. The volume fractions satisfy

$$\alpha_s + \alpha_g = 1. \tag{1.3}$$

We assume that the two fluids are stiffened such that each phase is characterized by an equation of state of the form, see [31]

$$\varepsilon_k = \frac{p_k + \gamma_k p_{\infty,k}}{\rho_k(\gamma_k - 1)}, \quad k = g, s. \tag{1.4}$$

The system (1.1)-(1.2) has the form of a system of balance laws in nonconservative form. A mathematical formulation of this kind of systems of balance laws was introduced in [13]. As well-known, the system (1.1)-(1.2) is not strictly hyperbolic as characteristic speeds coincide on certain sets, see [4, 35] for example. In particular, two characteristic speeds coincide everywhere: $\lambda_5 \equiv \lambda_7 \equiv u_s$. This corresponds to a linearly degenerate field and the associated contacts are called *solid contacts*. The system (1.1)-(1.2) shows its most complex structure around solid contacts, where the resonant phenomenon occurs and multiple solutions are available.

Often, the source terms in a system of nonconservative form may cause lots of inconveniences in approximating physical solutions of the system. Furthermore, standard numerical schemes for hyperbolic conservation laws may not work properly for approximating exact solutions of (1.1)-(1.2) when approximate states fall into a neighborhood of a region where characteristic speeds coincide and multiple exact solutions are available. This makes the topic of looking for a reliable numerical method for approximating solutions of (1.1)-(1.2) one of the most interesting computing problems.

Motivated by our earlier work [25, 38, 40] for simpler systems of balance laws in nonconservative form, we extend the argument and method in these works to build in this paper a well-balanced numerical scheme for (1.1)-(1.2), and then see what happen. The idea that is extended from these works to the present work is to use stationary contacts to "absorb" the source terms. First, we will transform the system to an equivalent form which consists of three "subsystems". The first subsystem consists of the governing

equations in the gas phase, the second subsystem consists of the conservation laws for the mixture, and the third subsystem is the compaction dynamics equation. Each subsystem will be dealt with separately due to its performance. For the first subsystem we absorb the source terms using stationary contacts in the gas phase. For the second subsystem of conservation laws of the mixture, we will apply a suitable scheme for conservation laws. This is different from the one in [40], where we keep the conservation of mass in the solid phase for this second subsystem. Observing that the solid velocity is constant across the solid contact, we employ the technique of Enquist-Osher scheme to discretize the third subsystem. Our numerical method is then proven to possess interesting properties: it can capture equilibrium states in the gas phase, it preserves the positivity of the volume fractions in both phases, it also preserves the positivity of the density in the gas phase. Moreover, we will show that our scheme also satisfies the numerical minimum entropy principle in the gas phase. We also provide various tests for data in both subsonic and supersonic regions, and comparisons with existing schemes. The scheme gives reasonably good results in supersonic regions that are not always treated in existing schemes, but does not give satisfactory results in the subsonic region. However, the scheme is robust.

Many authors have considered numerical approximations of systems of balance laws in nonconservative form. The reader is referred to [10, 26, 34, 32, 1, 23, 15, 3, 35, 2] and the references therein for works that aim at discretizing source terms in multi-phase flow models. In [39, 36] numerical methods for one-pressure models of two-phase flows were presented. In [18, 19, 8, 9, 5], numerical well-balanced schemes for a single conservation law with a source term are presented. In [25, 24] a well-balanced scheme for the model of fluid flows in a nozzle with variable cross-section was built and studied. Well-balanced schemes for one-dimensional shallow water equations were constructed in [5, 38, 12, 22, 33]. Related issues can be seen in [27, 28, 16, 37] for the study of the Riemann problem for the model of a fluid in a nozzle with discontinuous cross-sections, and in [29, 38, 7] for the study of Riemann problem for shallow water equations with discontinuous topography.

The organization of the paper is as follows. Section 2 provides us with backgrounds of the model. In Section 3 we investigate the jump relations for stationary waves and provide a computing strategy for these waves. In Section 4 we build the numerical scheme. Then, we prove that our scheme fully preserves the positivity of the volume fractions and the densities, and is partly well-balanced and satisfies the numerical entropy principle in the gas phase. Section 5 is devoted to numerical tests, where we show that our scheme can give a good approximation to the exact solution. Finally, in Section 6 we will draw remarks and conclusions.

2. Backgrounds

2.1. Stiffened gas equation of state

The stiffened gas dynamics equation of the form

$$p = (\gamma - 1)\rho(\varepsilon - \varepsilon_*) - \gamma p_\infty, \tag{2.1}$$

was presented in [31]. Recently, a very nice presentation of the thermodynamical variables and quantities for the stiffened gas equation of state was given by [14] in which they are obtained as functions of the two variables $(\rho, T), (\rho, e)$, or (p, T) . For our purposes in

the next sections, however, it is useful to express the thermodynamical variables and the specific enthalpy for the stiffened gas equation of state as a functions of (ρ, S).

As shown by [30], the Helmholtz free energy

$$Q(v,T) = \varepsilon - TS \tag{2.2}$$

is used to specify a complete equation of state. It follows from the thermodynamic identity

$$d\varepsilon = TdS - pdv \tag{2.3}$$

and (2.2) that

$$p(v,T) = -\partial_v Q, \quad S(v,T) = -\partial_T Q. \tag{2.4}$$

The Helmholtz free energy that is used to define the stiffened gas equation of state is given by

$$Q(v,T) = c_v T(1 - \ln(T/T_*) - (\gamma-1)\ln(v/v_*)) - S_* T + p_\infty v + \varepsilon_*, \tag{2.5}$$

where the parameters $c_v, \gamma, p_\infty, S_*, T_*, v_*$ and ε_* are constants specific to the fluid.

From (2.4) and (2.5), one obtains

$$p = (\gamma-1)c_v \frac{T}{v} - p_\infty, \tag{2.6}$$

and

$$S = c_v(\ln(T/T_*) + (\gamma-1)\ln(v/v_*)) + S_*. \tag{2.7}$$

Now, it follows from (2.7) that

$$T = T_* \left(\frac{v}{v_*}\right)^{1-\gamma} \exp\left(\frac{S-S_*}{c_v}\right),$$

which yields the temperature T as a function of (ρ, S):

$$T(\rho,S) = T_* \left(\frac{\rho}{\rho_*}\right)^{\gamma-1} \exp\left(\frac{S-S_*}{c_v}\right). \tag{2.8}$$

Substituting $T = T(\rho, S)$ from (2.8) to the expression of the pressure in (2.6) gives us

$$\begin{aligned} p(\rho,S) &= \frac{c_v(\gamma-1)T_*}{\rho_*^{\gamma-1}} \rho^\gamma \exp\left(\tfrac{S-S_*}{c_v}\right) - p_\infty \\ &= \kappa(S)\rho^\gamma - p_\infty, \end{aligned} \tag{2.9}$$

where

$$\kappa(S) := \frac{c_v(\gamma-1)T_*}{\rho_*^{\gamma-1}} \exp\left(\tfrac{S-S_*}{c_v}\right). \tag{2.10}$$

From (2.2) and (2.5), a straightforward calculation yields

$$\begin{aligned} \varepsilon &= Q(v,T) + TS \\ &= c_v T + p_\infty v + \varepsilon_*. \end{aligned} \tag{2.11}$$

Substituting the temperature from (2.8) into (2.11), we obtain the internal energy as a function of (ρ, S):

$$\varepsilon = \varepsilon(\rho, S) = c_v T_* \left(\frac{\rho}{\rho_*}\right)^{\gamma-1} \exp\left(\frac{S - S_*}{c_v}\right) + \frac{p_\infty}{\rho} + \varepsilon_*. \tag{2.12}$$

The specific enthalpy is defined by

$$h = \varepsilon + pv. \tag{2.13}$$

Substituting the internal energy $\varepsilon = \varepsilon(\rho, S)$ from (2.12) and the pressure $p = p(\rho, s)$ from (2.9) into (2.13), we obtain the specific enthalpy as a function of (ρ, S):

$$h(\rho, S) = \frac{\kappa(S)\gamma}{\gamma - 1}\rho^{\gamma-1} + \varepsilon_*, \tag{2.14}$$

where $\kappa(S)$ is defined by (2.10).

Taking the differentials both sides of (2.9) gives

$$\begin{aligned} dp &= \gamma\kappa(S)\rho^{\gamma-1} \exp\left(\tfrac{S-S_*}{c_v}\right) d\rho + \tfrac{1}{c_v}\kappa(S)\rho^\gamma \exp\left(\tfrac{S-S_*}{c_v}\right) dS \\ &= \tfrac{\gamma}{\rho}(p + p_\infty)d\rho + \tfrac{1}{c_v}(p + p_\infty)dS, \end{aligned}$$

where $\kappa(S)$ is defined by (2.10). From the last equation it holds that the square of the sound speed is given by

$$c^2 = \partial_S p(\rho, S) = \frac{\gamma(p + p_\infty)}{\rho}. \tag{2.15}$$

2.2. Characteristics

Let us denote the sound speeds by

$$c_k = \sqrt{\gamma_k(p_k + p_{\infty,k})/\rho_k}, \quad k = g, s. \tag{2.16}$$

Then, the eigenvalues of the system (1.1)-(1.2) are given by

$$\begin{aligned} &\lambda_1(U) = u_g - c_g, \quad \lambda_2(U) = u_g, \quad \lambda_3(U) = u_g + c_g, \\ &\lambda_4(U) = u_s - c_s, \quad \lambda_5(U) = u_s, \quad \lambda_6(U) = u_s + c_s, \\ &\lambda_7(U) = u_s. \end{aligned} \tag{2.17}$$

As well-known, the 1-, 3-, 4- and 6-characteristic fields are genuinely nonlinear, while the 2-, 5-, and 7-characteristic fields are linearly degenerate. The volume fractions change only across the 7-contacts, called the *solid contacts.* The Riemann invariants associated with the 7-characteristic field are $u_s, \kappa(S_g), \alpha_g\rho_g(u_s - u_g), \alpha_g p_g + \alpha_s p_s + \alpha_g\rho_g(u_s - u_g)^2$, and $\frac{(u_s-u_g)^2}{2} + h_g$, where $\kappa(S)$ is given by (2.10). Since

$$\lambda_5 = \lambda_7 = u_s$$

a solid contact may follows each 5-field or 7-field, or both. Moreover, λ_1 and λ_3 may coincide with λ_5. This makes the structure of Riemann solutions in any neighborhood of

a solid contact complicated. In particular, multiple solutions can be constructed. It is convenient to define the *subsonic region* as

$$\lambda_1(U) < \lambda_5(U) < \lambda_3(U)$$

and the *supersonic regions* as

$$\lambda_1(U) > \lambda_5(U) \quad \text{or} \quad \lambda_5(U) > \lambda_3(U).$$

3. Stationary contacts

The idea using stationary solutions to absorb source terms in the model of fluid flows in a nozzle was presented in [25]. Stationary discontinuities can be obtained as the limit of smooth stationary solutions, and they turn out to be the (stationary) contact discontinuities associated with the linearly characteristic field. Consequently, the associated contact waves are stationary and absorb the source terms. This helps to determine directly the interfacial states in any two consecutive cells. The interfacial states between two consecutive cells are also known as equilibrium states, which are resulted by stationary contacts associated with the characteristic field with zero characteristic speed.

We will develop in this work this approach for the model (1.1)-(1.2). However, interfacial states for the system (1.1)-(1.2) are the states of contact waves associated with the 7th characteristic field. These contacts propagate with speed u_s which do not create equilibrium states on the two sides of a node if $u_s \neq 0$. We therefore require that the stationary contacts are the ones associated with the 7th characteristic field and that $u_s \equiv 0$. Using the fact that Riemann invariants are constant across contact discontinuities, and then by letting $u_s = 0$, we can determine the algebraic equations for interfacial states. Nevertheless, we could start from the original requirement that source terms can be absorbed in stationary solutions. Then, we will show in the subsection 3.2 below that a stationary jump can be found as the limit of stationary smooth solutions. These stationary jumps turn out to be the stationary contacts associated with the 7th characteristic field when the solid velocity is zero. The algebraic equations for these stationary contacts are then used to evaluate interfacial states.

3.1. Equivalent system under separate forms

It is convenient to rewrite the system (1.1)-(1.2) as a combination of the following three subsystems. The first subsystem consists of equations of balance laws in the gas phase:

$$\begin{aligned}
&\partial_t(\alpha_g\rho_g) + \partial_x(\alpha_g\rho_g u_g) = 0,\\
&\partial_t(\alpha_g\rho_g u_g) + \partial_x(\alpha_g(\rho_g u_g^2 + p_g)) = p_g\partial_x\alpha_g,\\
&\partial_t(\alpha_g\rho_g e_g) + \partial_x(\alpha_g u_g(\rho_g e_g + p_g)) = -p_g u_s\partial_x\alpha_s.
\end{aligned} \tag{3.1}$$

It has the form of a conservation law with source terms

$$\partial_t v + \partial_x f(v) = s(v, \partial_x v),$$

where

$$v = \begin{pmatrix} \alpha_g\rho_g \\ \alpha_g\rho_g u_g \\ \alpha_g\rho_g e_g \end{pmatrix}, \quad f(v) = \begin{pmatrix} \alpha_g\rho_g u_g \\ (\alpha_g(\rho_g u_g^2 + p_g)) \\ (\alpha_g u_g(\rho_g e_g + p_g)) \end{pmatrix}, \quad s(v, \partial_x v) = \begin{pmatrix} 0 \\ p_g\partial_x\alpha_g \\ -p_g u_s\partial_x\alpha_s \end{pmatrix}.$$

The second subsystem consists of conservation laws of the mixture:

$$\begin{aligned}
&\partial_t(\alpha_g\rho_g + \alpha_s\rho_s) + \partial_x(\alpha_g\rho_g u_g + \alpha_s\rho_s u_s) = 0,\\
&\partial_t(\alpha_s\rho_s u_s + \alpha_g\rho_g u_g) + \partial_x\big(\alpha_s(\rho_s u_s^2 + p_s) + \alpha_g(\rho_g u_g^2 + p_g)\big) = 0,\\
&\partial_t(\alpha_s\rho_s e_s + \alpha_g\rho_g e_g) + \partial_x\big(\alpha_s u_s(\rho_s e_s + p_s) + \alpha_g u_g(\rho_g e_g + p_g)\big) = 0,
\end{aligned} \tag{3.2}$$

The third subsystem consists of only the compaction dynamics equation:

$$\partial_t\alpha_g + u_s\partial_x\alpha_g = 0. \tag{3.3}$$

3.2. The jump relations

First, let us consider the stationary smooth solutions of (1.1)-(1.2) in the gas phase which satisfy the following ordinary differential equations

$$\begin{aligned}
&(\alpha_g\rho_g u_g)' = 0,\\
&\big(\alpha_g(\rho_g u_g^2 + p_g)\big)' = p_g\alpha_g',\\
&\big(\alpha_g u_g(\rho_g e_g + p_g)\big)' = -p_g u_s\alpha_s',\\
&u_s\alpha_g' = 0, \quad x \in \mathbb{R},
\end{aligned} \tag{3.4}$$

subject to the initial data

$$U(x_0) = (\rho_g, u_g, p_g, \alpha_g)(x_0) = U_0.$$

The following lemma gives us a way to calculate stationary waves. The last equation in (3.4) implies that if the volume fractions change, i.e., $\alpha_g' \neq 0$, we have

$$u_s = 0.$$

Therefore, it holds at a stationary contact that

$$\lambda_5 = \lambda_7 = u_s = 0. \tag{3.5}$$

From (3.4) and (3.5) we obtain

$$\begin{aligned}
&(\alpha_g\rho_g u_g)' = 0,\\
&\big(\alpha_g(\rho_g u_g^2 + p_g)\big)' = p_g\alpha_g',\\
&\big(\alpha_g u_g(\rho_g e_g + p_g)\big)' = 0.
\end{aligned} \tag{3.6}$$

In the rest of this section, we deal with only the quantities in the gas phase. So we omit the subscript in the gas phase for simplicity.

Argued similarly as in [25], we can check that a solution of the following system is also a solution of (3.6) and therefore of (3.4):

$$\begin{aligned}
&(\alpha\rho u)' = 0,\\
&\left(\tfrac{u^2}{2} + h\right)' = 0,\\
&S' = 0,
\end{aligned} \tag{3.7}$$

where h is the enthalpy in the gas phase given by (2.14).

Lemma 3.1. *Across any stationary contact, the entropy in the gas phase is constant. The left-hand and right-hand states of a stationary contact in the gas phase satisfy*

$$\begin{aligned} &[\alpha\rho u] = 0, \\ &[\tfrac{u^2}{2} + h] = 0, \\ &[S] = 0, \end{aligned} \tag{3.8}$$

where $[S] := S^+ - S^-$*, and so on, denotes the difference between the right-hand and left-hand values of the variable.*

3.3. Characterization of roots of the nonlinear equations

It follows from Lemma 3.1 that a stationary contact in the gas phase of (1.1)-(1.2) connecting two states $U_0 = (\alpha_0, \rho_0, u_0)$ and $U = (\alpha, \rho, u)$ fulfils

$$\begin{aligned} &\alpha\rho u = \alpha_0\rho_0 u_0, \\ &\tfrac{u^2}{2} + h(\rho, S_0) = \tfrac{u_0^2}{2} + h(\rho_0, S_0). \end{aligned} \tag{3.9}$$

Now, let us fix one state $U_0 = (\alpha_0, \rho_0, u_0)$, and we will find all such states $U = (\alpha, \rho, u)$ that can be connected to by a stationary contact in the gas phase. Substituting $u = \alpha_0\rho_0 u_0/\alpha\rho$ from the first equation into the second equation of (3.9), we obtain the nonlinear algebraic equation

$$\frac{(\alpha_0\rho_0 u_0)^2}{2(\alpha\rho)^2} + h(\rho, S_0) = \frac{u_0^2}{2} + h(\rho_0, S_0), \tag{3.10}$$

where

$$h(\rho, S) = \frac{\kappa(S)\gamma}{\gamma - 1}\rho^{\gamma-1} + \varepsilon_*, \quad \kappa(S) = \frac{c_v(\gamma-1)T_*}{\rho_*^{\gamma-1}} \exp\left(\frac{S - S_*}{c_v}\right).$$

As in [28], re-arranging terms of (3.10), we obtain the following equation

$$F(U_0, \rho, \alpha) := \mathrm{sgn}(u_0)\Big(u_0^2 - \frac{2\kappa\gamma}{\gamma-1}(\rho^{\gamma-1} - \rho_0^{\gamma-1})\Big)^{1/2}\rho - \frac{\alpha_0 u_0 \rho_0}{\alpha} = 0, \quad \kappa := \kappa(S_0). \tag{3.11}$$

The strategy of finding the stationary contacts between the given fixed state $U_0 = (\alpha_0, \rho_0, u_0)$ and $U = (\alpha, \rho, u)$ now is that we resolve the density ρ and then the velocity u in terms of the volume fraction α. More precisely, the volume fraction α will play the role of a parameter, the density ρ will be found by solving the algebraic equation (3.11), and then the velocity will be given by the first equation in (3.9). Thus, the values of ρ will be the zeros of the function $F(U_0, \rho, \alpha)$. We have

$$F(U_0, \rho = 0, a) = F(U_0, \rho = \bar{\rho}, a) = -\frac{\alpha_0 u_0 \rho_0}{\alpha},$$

which has the same sign as $-u_0$, and

$$\frac{\partial F(U_0, \rho; \alpha)}{\partial \rho} = \frac{u_0^2 - \frac{2\kappa\gamma}{\gamma-1}(\rho^{\gamma-1} - \rho_0^{\gamma-1}) - \kappa\gamma\rho^{\gamma-1}}{\Big(u_0^2 - \frac{2\kappa\gamma}{\gamma-1}(\rho^{\gamma-1} - \rho_0^{\gamma-1})\Big)^{1/2}}.$$

Set

$$\begin{aligned}\bar{\rho}(U_0) &= \left(\tfrac{\gamma-1}{2\kappa\gamma}u_0^2 + \rho_0^{\gamma-1}\right)^{\frac{1}{\gamma-1}},\\ \rho_{\max}(\rho_0,u_0) &= \left(\tfrac{\gamma-1}{\kappa\gamma(\gamma+1)}u_0^2 + \tfrac{2}{\gamma+1}\rho_0^{\gamma-1}\right)^{\frac{1}{\gamma-1}}.\end{aligned} \tag{3.12}$$

By a similar argument as in [40], we can see that the function $\rho \mapsto F(U_0,\rho,\alpha)$ is defined on the interval

$$0 \le \rho \le \bar{\rho}(U_0).$$

Furthermore, if $u_0 > 0$ ($u_0 < 0$), then the function $\rho \mapsto F(U_0,\rho,\alpha)$ is strictly increasing (strictly decreasing, respectively) for $0 \le \rho \le \rho_{\max}(\rho_0,u_0)$, and strictly decreasing (strictly increasing, respectively) for $\rho_{\max}(\rho_0,u_0) \le \rho \le \bar{\rho}(U_0)$, where $\rho_{\max}(\rho_0,u_0)$ is defined by (3.12).

Set

$$\begin{aligned}G_1 &:= \{(\alpha,\rho,u) \,:\, u < -\sqrt{p'(\rho)}\},\\ G_2 &:= \{(\alpha,\rho,u) \,:\, |u| < \sqrt{p'(\rho)}\},\\ G_2^+ &:= \{(\alpha,\rho,u) \,:\, 0 < u < \sqrt{p'(\rho)}\},\\ G_2^- &:= \{(\alpha,\rho,u) \,:\, 0 > u > -\sqrt{p'(\rho)}\},\\ G_3 &:= \{(\alpha,\rho,u) \,:\, u > \sqrt{p'(\rho)}\},\\ \mathcal{C} &:= \{(\alpha,\rho,u) \,:\, u = \pm\sqrt{p'(\rho)}\}.\end{aligned} \tag{3.13}$$

Arguing similarly as in [28, 37], we can characterize the roots of the nonlinear equation (3.11) as follows.

Proposition 3.2. *The nonlinear equation for the gas density (3.11), and therefore the equation (3.10), admits exactly two roots, denoted by $\varphi_1(U_0,\alpha) < \varphi_2(U_0,\alpha)$ whenever*

$$\alpha > \alpha_{\min}(U_0) := \frac{\alpha_0\rho_0|u_0|}{\sqrt{\kappa\gamma}\,\rho_{\max}^{\frac{\gamma+1}{2}}(\rho_0,u_0)}. \tag{3.14}$$

Moreover, if $\alpha = \alpha_{\min}(U_0)$, then $\varphi_1(U_0,\alpha) = \varphi_2(U_0,\alpha)$. The location of these roots can be described as follows. If $\alpha > \alpha_0$, then

$$\varphi_1(U_0,\alpha) < \rho_0 < \varphi_2(U_0,\alpha).$$

If $\alpha < \alpha_0$, then

$$\begin{aligned}&\rho_0 < \varphi_1(U_0,\alpha) \quad \textit{for} \quad U_0 \in G_1 \cup G_3,\\ &\rho_0 > \varphi_2(U_0,\alpha) \quad \textit{for} \quad U_0 \in G_2.\end{aligned}$$

Moreover, given $U = (\alpha,\rho,u)$ and let $\alpha_{\min}(U)$ be defined as in (3.14). By a similar argument as in [28], one obtains the following conclusions

$$\begin{aligned}&\alpha_{\min}(U) < \alpha, \quad U \in G_i,\ i = 1,2,3,\\ &\alpha_{\min}(U) = \alpha, \quad U \in \mathcal{C},\\ &\alpha_{\min}(U) = 0, \quad \rho = 0 \quad \text{or} \quad u = 0.\end{aligned} \tag{3.15}$$

3.4. Monotonicity Criterion

It is derived from Proposition 3.2 that there are possibly multiple stationary contacts issuing from a given state U_0 and reaching a state with a new volume fraction α. To select a unique stationary wave, we need the following so-called Monotonicity criterion. The first equation in (3.8) also defines a curve $\rho \mapsto \alpha = \alpha(U_0, \rho)$. So we require that

MONOTONICITY CRITERION. *Along any stationary wave, the volume fraction $\alpha = \alpha(U_0, \rho)$ must be monotone as a function of ρ.*

A similar criterion was used in [28, 25, 40, 20, 21]. The Monotonicity Criterion enables us to selectly geometrically the admissible stationary contacts as follows.

Lemma 3.3. *The Monotonicity Criterion is equivalent to saying that any stationary shock does not cross the boundary $\mathcal{C}$. In other words:*

(i) If $U_0 \in G_1 \cup G_3$, then only the zero $\rho = \varphi_1(U_0, \alpha)$ is selected.

(ii) If $U_0 \in G_2$, then only the zero $\rho = \varphi_2(U_0, \alpha)$ is selected.

3.5. Computing strategy

The advantages of selecting the function F as in (3.11) are that its zeros can be characterized, as indicated in the above argument. However, for the computing purposes, it may be more convenient to look for another candidate. This is because the function F might not be convex, making it hard to apply the Newton-Raphson method to find the roots. To deal with computing purposes, we re-write the equation (3.10) as follows. Multiplying both sides of (3.10) by ρ and re-arranging terms, we obtain the following equation

$$\mu(S)(\rho^\gamma - \rho_0^{\gamma-1}\rho) + \frac{u_0^2}{2}\left(\frac{\alpha_0^2\rho_0^2}{\alpha^2\rho} - \rho\right) = 0, \tag{3.16}$$

where

$$\mu(S) := \frac{\gamma c_v T_*}{\rho_*^{\gamma-1}} \exp\left(\frac{S - S_*}{c_v}\right).$$

It is easy to see that

$$\mu(S) = \frac{\gamma}{\gamma - 1}\kappa(S),$$

where $\kappa(S)$ is defined by (2.10). Since the entropy is constant across a stationary contact, i.e., $S = S_0$, the equation (3.16) becomes

$$\Phi(\rho) := \mu(\rho^\gamma - \rho_0^{\gamma-1}\rho) + \frac{u_0^2}{2}\left(\frac{\alpha_0^2\rho_0^2}{\alpha^2\rho} - \rho\right) = 0, \tag{3.17}$$

where

$$\mu := \mu(S_0) = \frac{\gamma c_v T_*}{\rho_*^{\gamma-1}} \exp\left(\frac{S_0 - S_*}{c_v}\right) > 0.$$

We will see that the function $\rho \mapsto \Phi(\rho)$ has advantages for computing purposes. Indeed, a straightforward calculation gives

$$\begin{aligned} &\Phi'(\rho) = \mu(\gamma\rho^{\gamma-1} - \rho_0^{\gamma-1}) - \tfrac{u_0^2}{2}\left(\tfrac{\alpha_0^2\rho_0^2}{\alpha^2\rho^2} + 1\right), \\ &\Phi"(\rho) = \mu\gamma(\gamma-1)\rho^{\gamma-2} + \tfrac{u_0^2\alpha_0^2\rho_0^2}{\alpha^2\rho^3} > 0. \end{aligned} \tag{3.18}$$

The second line of (3.18) shows that the function $\rho \mapsto \Phi(\rho)$ is strictly convex. The use of Newton-Raphson method is thus convenient for finding roots of the nonlinear equation (3.17) and therefore finding stationary contacts. In this case it is convenient to take the initial guess ρ^0 for the Newton-Raphson method such that $\Phi(\rho^0) > 0$.

We still need to determine a computing strategy to find the roots of (3.17), in view of the Monotonicity Criterion. Now it holds that

$$\begin{aligned} &\Phi(\rho) \to +\infty, \quad \rho \to 0, \rho \to \infty \\ &\Phi(\rho_0) = \tfrac{u_0^2}{2}\rho_0(\tfrac{\alpha_0^2}{\alpha^2} - 1) > 0 \quad \text{iff} \quad \alpha < \alpha_0. \end{aligned} \tag{3.19}$$

It is derived from (3.19), Proposition 3.2 and Lemma 3.3 and that the admissible stationary contact can be chosen using the Newton-Raphson method. Precisely, we get the following result.

Lemma 3.4. *The Newton-Raphson method for the nonlinear equation (3.17) generates a sequence of approximate solutions which converges to the admissible root in the sense that this root is the ρ-component of a stationary contact satisfying the Monotonicity Criterion if the initial guess ρ^0 for the method is taken in the following way:*

(i) Case 1: $U_0 \in G_1 \cup G_3$: if $\alpha < \alpha_0$, then we can take $\rho^0 = \rho_0$; if $\alpha > \alpha_0$, we can take $\rho^0 < \rho_0$ such that $\Phi(\rho^0) > 0$; in this case the sequence then converges to the root $\rho = \varphi_1(U_0, \alpha)$.

(ii) Case 2: $U_0 \in G_2$: if $\alpha < \alpha_0$, then we can take $\rho^0 = \rho_0$; if $\alpha > \alpha_0$, we can take $\rho^0 > \rho_0$ such that $\Phi(\rho^0) > 0$; in this case the sequence then converges to the root $\rho = \varphi_2(U_0, \alpha)$.

4. A well-balanced scheme based on stationary waves

Given a uniform time step Δt, and a spacial mesh size Δx, setting $x_j = j\Delta x, j \in \mathbf{Z}$, and $t_n = n\Delta t, n \in \mathbf{N}$, we denote U_j^n to be an approximation of the exact value $U(x_j, t_n)$. A C.F.L condition is also required on the mesh sizes:

$$\theta \max_U\{|\lambda_i(U)|, i = 1, 2, 3, 4, 5, 6, 7\} < 1, \quad \theta := \frac{\Delta t}{\Delta x}. \tag{4.1}$$

4.1. Numerical treatment of the first subsystem (3.1)

To discretize the first subsystem (3.1), we use the following strategy which consists of two steps:

Step 1. First, the volume fraction change creates a stationary contact, which absorbs the nonconservative term $p_g\partial_x\alpha_g$;

Step 2. Second, the stationary contact moves and obeys the governing equation where the volume fraction is constant. This enables us to eliminate the volume fraction on both sides of the equations so that the subsystem becomes the usual gas dynamics.

Assume that the volume fraction is constant, then, the subsystem (3.1) becomes the usual gas dynamics equations

$$\partial_t v + \partial_x f_1(v) = 0,$$

where

$$v := \begin{pmatrix} \rho_g \\ \rho_g u_g \\ \rho_g e_g \end{pmatrix}, \quad f_1(v) := \begin{pmatrix} \rho_g u_g \\ \rho_g u_g^2 + p_g \\ u_g(\rho_g e_g + p_g) \end{pmatrix}.$$

Let $g(v, w)$ be a suitable standard numerical flux $g_1(v, w)$ for the usual gas dynamic equations. For $j \in \mathbf{Z}, n = 0, 1, 2, 3, ...$, we set

$$v_j^n = \begin{pmatrix} \rho_{g,j}^n \\ \rho_{g,j}^n u_{g,j}^n \\ \rho_{g,j}^n e_{g,j}^n \end{pmatrix}, \quad v_{j,+}^n = \begin{pmatrix} \rho_{g,j,+}^n \\ \rho_{g,j,+}^n u_{g,j,+}^n \\ \rho_{g,j,+}^n e_{g,j,+}^n \end{pmatrix}, \quad v_{j,-}^n = \begin{pmatrix} \rho_{g,j,-}^n \\ \rho_{g,j,-}^n u_{g,j,-}^n \\ \rho_{g,j,-}^n e_{g,j,-}^n \end{pmatrix},$$

where

$$e_{g,j,+}^n = \varepsilon\big(\rho_{g,j,+}^n, S_{g,j}^n\big) + \frac{(u_{g,j,+}^n)^2}{2},$$
$$e_{g,j,-}^n = \varepsilon\big(\rho_{g,j,-}^n, S_{g,j}^n\big) + \frac{(u_{g,j,-}^n)^2}{2},$$

and the quantities $\rho_{g,j,\pm}^n, u_{g,j,\pm}^n$ will be given below. The first component of the well-balanced scheme is defined by

$$v_j^{n+1} = v_j^n - \theta(g_1(v_j^n, v_{j+1,-}^n) - g_1(v_{j-1,+}^n, v_j^n)), \quad j \in \mathbf{Z}, n = 0, 1, 2, ..., \tag{4.2}$$

where the state $v_{j+1,-}^n$ is known if the values $\rho_{g,j+1,-}^n, u_{g,j+1,-}^n$ are known, and the state $v_{j-1,+}^n$ is known if the values $\rho_{g,j-1,+}^n, u_{g,j-1,+}^n$ are known, $j \in \mathbf{Z}, n \in \mathbf{N}$. Let us now describe the way to compute $v_{j+1,-}^n$. To find the values $\rho_{g,j+1,-}^n, u_{g,j+1,-}^n$, $j \in \mathbf{Z}, n \in \mathbf{N}$, we use an "absorbing volume fraction change" process using stationary contacts as said earlier in Step 1 above. Moreover, to ensure that the volume fraction change will always give a stationary contact, we propose to define a "relaxation" value, which can be seen as an approximate value in general, for the volume fraction

$$\alpha_{g,j}^{n,\text{Relax}} = \max\{\alpha_{g,j}^n, \alpha_{\min}(\alpha_{g,j+1}^n, \rho_{g,j+1}^n, u_{g,j+1}^n)\}, \tag{4.3}$$

where the quantity $\alpha_{\min}$ is defined by (3.14). This argument and (3.8) mean that these values satisfy the relations

$$\begin{aligned} &\alpha_{g,j}^{n,\text{Relax}} \rho_{g,j+1,-}^n u_{g,j+1,-}^n = \alpha_{g,j+1}^n \rho_{g,j+1}^n, u_{g,j+1}^n, \\ &\tfrac{(u_{g,j+1,-}^n)^2}{2} + h(\rho_{g,j+1,-}^n, S_{g,j+1}^n) = \tfrac{(u_{g,j+1}^n)^2}{2} + h(\rho_{g,j+1}^n, S_{g,j+1}^n), \\ &S_{g,j+1,-}^n = S_{g,j+1}^n. \end{aligned} \tag{4.4}$$

Hence, in accordance with the observations in the previous section, the value $\rho_{g,j+1,-}^n$ is calculated by taking

$$\rho_{g,j+1,-}^n = \varphi_i(U_{g,j+1}^n, \alpha_{g,j}^{n,\text{Relax}}), \quad U_{g,j+1}^n := (\alpha_{g,j+1}^n, \rho_{g,j+1}^n, u_{g,j+1}^n), \quad i = 1, 2, \tag{4.5}$$

where the index i is selected in accordance with Lemma 3.3.

Furthermore, it is derived from Lemma 3.4 that if the Newton-Raphson method for solving the nonlinear equation (3.17) is chosen with the initial guess ρ^0, the procedure finding $\rho^n_{g,j+1,-}$ can be described as follows.

(i) Assume that the point $(\rho^n_{g,j+1}, u^n_{g,j+1})$ belongs to either the lower region G_1 or the upper region G_3 in the (ρ, u)-plane defined by (3.13). If $\alpha = \alpha^n_{g,j+1} < \alpha_0 = \alpha^{n,\text{Relax}}_{g,j}$, then we can take $\rho^0 = \rho^n_{g,j+1}$. If $\alpha = \alpha^n_{g,j+1} > \alpha_0 = \alpha^{n,\text{Relax}}_{g,j}$, we can take $\rho^0 < \rho^n_{g,j+1}$ such that $\Phi(\rho^0) > 0$. (This means that the value $\varphi_1(\alpha^n_{g,j+1}, \rho^n_{g,j+1}, u^n_{g,j+1}, \alpha^{n,\text{Relax}}_{g,j})$ will be found).

(ii) Assume that the point $(\rho^n_{g,j+1}, u^n_{g,j+1})$ belongs to the middle region G_2 in the (ρ, u)-plane defined by (3.13). If $\alpha = \alpha^n_{g,j+1} < \alpha_0 = \alpha^{n,\text{Relax}}_{g,j}$, then we can take $\rho^0 = \rho^n_{g,j+1}$. If $\alpha = \alpha^n_{g,j+1} > \alpha_0 = \alpha^{n,\text{Relax}}_{g,j}$, we can take $\rho^0 > \rho^n_{g,j+1}$ such that $\Phi(\rho^0) > 0$. (This means that the value $\varphi_2(\alpha^n_{g,j+1}, \rho^n_{g,j+1}, u^n_{g,j+1}, \alpha^{n,\text{Relax}}_{g,j})$ will be found).

Then, the value $u^n_{g,j+1,-}$ is calculated using the second equation of (4.4) as:

$$u^n_{g,j+1,-} = \frac{\alpha^n_{g,j+1}\rho^n_{g,j+1}u^n_{g,j+1}}{\alpha^{n,\text{Relax}}_{g,j}\rho^n_{g,j+1,-}}.$$

Similarly, we compute the state $v^n_{j-1,+}$ by first defining a "relaxation" value for the volume fraction

$$\alpha^{n,\text{Relax}}_{g,j} = \max\{\alpha^n_{g,j}, \alpha_{\min}(\alpha^n_{g,j-1}, \rho^n_{g,j-1}, u^n_{g,j-1})\}. \tag{4.6}$$

We also require that the corresponding values of the stationary contact satisfy the relations

$$\begin{aligned} &\alpha^{n,\text{Relax}}_{g,j}\rho^n_{g,j-1,+}u^n_{g,j-1,+} = \alpha^n_{g,j-1}\rho^n_{g,j-1}, u^n_{g,j-1}, \\ &\tfrac{(u^n_{g,j-1,+})^2}{2} + h(\rho^n_{g,j-1,+}, S^n_{g,j-1}) = \tfrac{(u^n_{g,j-1})^2}{2} + h(\rho^n_{g,j-1}, S^n_{g,j-1}), \\ &S^n_{g,j-1,+} = S^n_{g,j-1}. \end{aligned} \tag{4.7}$$

The value $\rho^n_{g,j-1,+}$ is therefore calculated by taking

$$\rho^n_{g,j-1,+} = \varphi_i(U^n_{g,j-1}, \alpha^{n,\text{Relax}}_{g,j}), \quad U^n_{g,j-1} := (\alpha^n_{g,j-1}, \rho^n_{g,j-1}, u^n_{g,j-1}), \quad i = 1, 2, \tag{4.8}$$

where the index i is selected in accordance with Lemma 3.3.

Again, it is derived from Lemma 3.4 that if the Newton-Raphson method for solving the nonlinear equation (3.17) is chosen with the initial guess ρ^0, the procedure finding $\rho^n_{g,j-1,+}$ can be described as follows.

(iii) Assume that the point $(\rho^n_{g,j-1}, u^n_{g,j-1})$ belongs to either the lower region G_1 or the upper region G_3 in the (ρ, u)-plane defined by (3.13). If $\alpha = \alpha^n_{g,j-1} < \alpha_0 = \alpha^{n,\text{Relax}}_{g,j}$, then we can take $\rho^0 = \rho^n_{g,j-1}$. If $\alpha = \alpha^n_{g,j-1} > \alpha_0 = \alpha^{n,\text{Relax}}_{g,j}$, we can take $\rho^0 < \rho^n_{g,j-1}$ such that $\Phi(\rho^0) > 0$. (This means that the value $\varphi_1(\alpha^n_{g,j-1}, \rho^n_{g,j-1}, u^n_{g,j-1}, \alpha^{n,\text{Relax}}_{g,j})$ is found).

(iv) Assume that the point $(\rho^n_{g,j-1}, u^n_{g,j-1})$ belongs to the middle region G_2 in the (ρ, u)-plane defined by (3.13). If $\alpha = \alpha^n_{g,j-1} < \alpha_0 = \alpha^{n,\mathrm{Relax}}_{g,j}$, then we can take $\rho^0 = \rho^n_{g,j-1}$. If $\alpha = \alpha^n_{g,j-1} > \alpha_0 = \alpha^{n,\mathrm{Relax}}_{g,j}$, we can take $\rho^0 > \rho^n_{g,j-1}$ such that $\Phi(\rho^0) > 0$. (This means that the value $\varphi_2(\alpha^n_{g,j-1}, \rho^n_{g,j-1}, u^n_{g,j-1}, \alpha^{n,\mathrm{Relax}}_{g,j})$ is found).

Finally, the value $u = u^n_{g,j-1,+}$ is computed using the second equation of (4.7) as:

$$u^n_{g,j-1,+} = \frac{\alpha^n_{g,j-1}\rho^n_{g,j-1}u^n_{g,j-1}}{\alpha^{n,\mathrm{Relax}}_{g,j}\rho^n_{g,j-1,+}}.$$

4.2. Numerical treatment of the second subsystem (3.2)

We now turn to deal with the second subsystem (3.2) which has the conservative form:

$$\partial_t w + \partial_x f_2(w) = 0,$$

where

$$w := \begin{pmatrix} \alpha_g\rho_g + \alpha_s\rho_s \\ \alpha_g\rho_g u_g + \alpha_s\rho_s u_s \\ \alpha_g\rho_g e_g + \alpha_s\rho_s e_s \end{pmatrix}, \quad f_2(w) := \begin{pmatrix} \alpha_g\rho_g u_g + \alpha_s\rho_s u_s \\ \alpha_g(\rho_g u_g^2 + p_g) + \alpha_s(\rho_s u_s^2 + p_s) \\ \alpha_g u_g(\rho_g e_g + p_g) + \alpha_s u_s(\rho_s e_s + p_s). \end{pmatrix}.$$

Naturally, a conservative scheme can be applied to (3.2):

$$w^{n+1}_j = w^n_j - \theta(g_2(w^n_j, w^n_{j+1}) - g_2(w^n_{j-1}, w^n_j)), \quad j \in \mathbf{Z}, n = 0, 1, 2, ... \tag{4.9}$$

For example, we may take a scheme involving the unknown function and the flux function only such as the Lax-Friedrichs scheme, the Lax-Wendroff scheme, or Richtmyer's scheme, etc.

4.3. Numerical treatment of the third subsystem (3.3)

Finally, we consider the numerical treatment for the third subsystem, which contains only the compaction dynamics equation (1.2). The discretization of the compaction dynamics equation is motivated by the very interesting fact that among elementary waves, the volume fractions change only across the solid contacts associated with the characteristic speed $\lambda_7 = u_s$, see [4, 35] for example. Moreover, the solid velocity is constant across a solid contact. This suggests that the nonconservative term $u_s\partial_x\alpha_g$ may have more regularity property than it seems and furthermore it can be discretized using the upwind scheme. Thus, we apply the Engquist-Osher scheme for the compaction dynamics equation (1.2):

$$\alpha^{n+1}_{g,j} = \alpha^n_{g,j} - \theta\Big(u^{n,+}_{s,j}(\alpha^n_{g,j} - \alpha^n_{g,j-1}) + u^{n,-}_{s,j}(\alpha^n_{g,j+1} - \alpha^n_{g,j})\Big), \tag{4.10}$$

where $\theta = \Delta t/\Delta x$, and

$$u^{n,+}_{s,j} := \max\{u^n_{s,j}, 0\}, \quad u^{n,-}_{s,j} := \min\{u^n_{s,j}, 0\}, \quad j \in \mathbf{Z}, n = 0, 1, 2, 3, ...$$

In studying our above numerical method, for definitiveness, we may take both numerical fluxes in (4.2) and (4.9) to be the Lax-Friedrichs. In this case, it reads

$$\begin{array}{l} v_j^{n+1} = \frac{1}{2}(v_{j+1,-}^n + v_{j-1,+}^n) - \frac{\theta}{2}(f_1(v_{j+1,-}^n) - f_1(v_{j-1,+}^n)), \\ w_j^{n+1} = \frac{1}{2}(w_{j+1}^n + w_{j-1}^n) - \frac{\theta}{2}(f_2(w_{j+1}^n) - f_2(w_{j-1}^n)), \end{array} \tag{4.11}$$

for $j \in \mathbf{Z}, n = 0, 1, 2, ...$

The following theorem provides first remarkable properties of our scheme.

Theorem 4.1. *(i) (*Fully preserving positivity of volume fractions*) Our scheme (4.1)-(4.10) preserves the positivity of the volume fractions. This means that if $\alpha_{k,j}^0 > 0$ for all $j \in \mathbf{Z}$, then $\alpha_{k,j}^n > 0$ for all $j \in \mathbf{Z}, n = 1, 2, 3, ..., k = s, g$.*

*(ii) (*Partly well-balanced scheme*) Our scheme (4.1)-(4.10) captures exactly equilibrium states in the gas phase.*

Proof. (i) Since $\alpha_s + \alpha_g = 1$, it is sufficient to show that $0 < \alpha_{g,j}^{n+1} < 1$ whenever $0 < \alpha_{g,j}^n < 1, j \in \mathbf{Z}$. Let $0 < \alpha_{g,j}^n < 1, j \in \mathbf{Z}$. For simplicity we drop the index g in the gas volume fraction, and the index s in the solid velocity. First, consider the case $u_j^n \geq 0$. It holds that

$$\begin{array}{rl} \alpha_j^{n+1} & = \alpha_j^n - \theta u_j^n(\alpha_j^n - \alpha_{j-1}^n) \\ & = \alpha_j^n(1 - \theta u_j^n) + \theta u_j^n \alpha_{j-1}^n. \end{array}$$

It follows from the C.F.L. condition that both $0 \leq (1 - \theta u_j^n) \leq 1$ and $0 \leq \theta u_j^n \leq 1$. So, from the last equality we deduce that

$$0 < \alpha_j^{n+1} = \alpha_j^n(1 - \theta u_j^n) + \theta u_j^n \alpha_{j-1}^n \leq \max\{\alpha_j^n, \alpha_{j-1}^n\} < 1. \tag{4.12}$$

Similarly, consider now the case $u_j^n < 0$. Then,

$$\begin{array}{rl} \alpha_j^{n+1} & = \alpha_j^n - \theta u_j^n(\alpha_{j+1}^n - \alpha_j^n) \\ & = \alpha_j^n(1 + \theta u_j^n) - \theta u_j^n \alpha_{j+1}^n. \end{array}$$

The C.F.L. condition also gives $0 \leq (1 + \theta u_j^n) \leq 1$ and $0 \leq -\theta u_j^n \leq 1$. Thus, the last equality yields

$$0 < \alpha_j^{n+1} = \alpha_j^n(1 + \theta u_j^n) - \theta u_j^n \alpha_{j-1}^n \leq \max\{\alpha_j^n, \alpha_{j+1}^n\} < 1. \tag{4.13}$$

From (4.12) and (4.13) we obtain (i).

(ii) Let us be given a stationary contact. Then, the entropy in the gas phase is constant, and so

$$\begin{array}{l} \alpha_{g,j+1}^n \rho_{g,j+1}^n u_{g,j+1}^n = \alpha_{g,j}^n \rho_{g,j}^n u_{g,j}^n, \\ \frac{(u_{g,j+1}^n)^2}{2} + h_g(\rho_{g,j+1}^n) = \frac{(u_{g,j}^n)^2}{2} + h_g(\rho_{g,j}^n). \end{array} \tag{4.14}$$

The equations (4.14) imply that

$$\begin{array}{ll} \rho_{g,j+1,-}^n = \rho_{g,j}^n, & u_{g,j+1,-}^n = u_{g,j}^n, \\ \rho_{g,j-1,+}^n = \rho_{g,j}^n, & u_{g,j-1,+}^n = u_{g,j}^n, \end{array}$$

so that

$$v^n_{j+1,-} = v^n_j, \quad v^n_{j-1,+} = v^n_j.$$

This yields

$$v^{n+1}_j = v^n_j. \tag{4.15}$$

The identity (4.15) establishes (ii). The proof of Theorem 4.1 is complete. □

The following theorem provides us with other important properties of our scheme (4.1)-(4.10) with the specific choice of the Lax-Friedrichs flux (4.11).

Theorem 4.2. *(i) (*Preserving positivity of gas density*) Our scheme (4.1)-(4.11) preserves the positivity of the density in the gas phase under the assumptions that*

$$1 < \gamma_g < 2, \tag{4.16}$$

and

$$\theta \max_U\{|\lambda_i(U)|, i = 1, 2, 3, 4, 5, 6, 7\} < \frac{1}{\sqrt{2}}, \quad \theta = \frac{\Delta t}{\Delta x}. \tag{4.17}$$

This means that if $\rho^0_{k,j} > 0$ for all $j \in \mathbf{Z}$, then $\rho^n_{k,j} > 0$ for all $j \in \mathbf{Z}, n = 1, 2, 3, ..., k = s, g$.

*(ii) (*Partly numerical minimum entropy principle*) Assume that the conditions (4.16) and (4.17) are fulfilled. Then, our scheme (4.1)-(4.11) satisfies the following* minimum entropy principle *in the gas phase:*

$$S^{n+1}_{g,j} \geq \min\{S^n_{g,j-1}, S^n_{g,j+1}\}, \quad j \in \mathbf{Z}, n = 0, 1, 2, 3, ... \tag{4.18}$$

Proof. For simplicity we drop the subscript index of the phase.

(i) It is sufficient to show that for any given integer n, if $\rho^n_j > 0$ for j, then $\rho^{n+1}_j > 0$ for all j. Let us take an arbitrary and fixed, non-negative integer n. Assume now that $\rho^n_j > 0, \forall j \in \mathbf{Z}$. It holds that

$$\begin{aligned} \rho^{n+1}_j &= \tfrac{\rho^n_{j-1,+}+\rho^n_{j+1,-}}{2} + \tfrac{\theta}{2}(\rho^n_{j-1,+}u^n_{j-1,+} - \rho^n_{j+1,-}u^n_{j+1,-}) \\ &\geq \tfrac{\rho^n_{j-1,+}+\rho^n_{j+1,-}}{2} - \tfrac{\theta}{2}\max\{|u^n_{j-1,+}|, |u^n_{j+1,-}|\}(\rho^n_{j-1,+} + \rho^n_{j+1,-}) \\ &\geq \tfrac{\rho^n_{j-1,+}+\rho^n_{j+1,-}}{2}\left(1 - \theta\max\left(|u^n_{j-1,+}|, |u^n_{j+1,-}|\right)\right). \end{aligned} \tag{4.19}$$

It follows from Lemma 3.3 that

$$\rho^n_{j,\pm} > 0, \quad j \in \mathbf{Z}.$$

Thus, it is derived from (4.19) that to demonstrate the positivity of the density, we remain to point out that

$$\theta\max\{|u^n_{j-1,+}|, |u^n_{j+1,-}|\} < 1. \tag{4.20}$$

It follows from (2.14) and the condition (4.16) that

$$\begin{aligned} h_\rho(\rho, S) &= \tfrac{(\gamma-1)\gamma c_v T_*}{\rho_*^{\gamma-1}}\rho^{\gamma-2}\exp\left(\tfrac{S-S_*}{c_v}\right) > 0, \\ h_{\rho\rho}(\rho, S) &= \tfrac{(\gamma-2)(\gamma-1)\gamma c_v T_*}{\rho_*^{\gamma-1}}\rho^{\gamma-3}\exp\left(\tfrac{S-S_*}{c_v}\right) < 0, \end{aligned}$$

which imply that the function $\rho \mapsto h(\rho, S)$ is strictly increasing and strictly concave for each fixed entropy S. Hence,

$$\begin{aligned}\tfrac{1}{2}(u^n_{j+1})^2 - \tfrac{1}{2}(u^n_{j+1,-})^2 &= h(\rho^n_{j+1,-}, S^n_{j+1}) - h(\rho^n_{j+1}, S^n_{j+1}) \\ &\geq h_\rho(\rho^n_{j+1}, S^n_{j+1})(\rho^n_{j+1,-} - \rho^n_{j+1}) \\ &= \tfrac{p_\rho(\rho^n_{j+1}, S^n_{j+1})}{\rho^n_{j+1}}(\rho^n_{j+1,-} - \rho^n_{j+1}) \\ &= p_\rho(\rho^n_{j+1}, S^n_{j+1})\Big(\tfrac{\rho^n_{j+1,-}}{\rho^n_{j+1}} - 1\Big) \geq -p_\rho(\rho^n_{j+1}, S^n_{j+1}).\end{aligned}$$

Using the last inequality, Lemma 3.1 and the condition (4.17), we obtain

$$\begin{aligned}|u^n_{j+1,-}| &\leq \sqrt{(u^n_{j+1})^2 + 2p_\rho(\rho^n_{j+1}, S^n_{j+1})} \\ &< \sqrt{2}(|u^n_{j+1}| + \sqrt{p_\rho(\rho^n_{j+1}, S^n_{j+1})}) \\ &= \sqrt{2}\lambda_3(U^n_{j+1}) \\ &\leq \sqrt{2}\max_U\{\lambda_i(U), i = 1,2,3,4,5,6,7\} \leq \tfrac{1}{\theta}.\end{aligned} \tag{4.21}$$

Similarly,

$$|u^n_{j-1,+}| < \frac{1}{\theta}. \tag{4.22}$$

From (4.21) and (4.22), we obtain (4.20). This establishes (i).

(ii) Let $v = 1/\rho$ be the specific volume. We will first show that the gas is in a local thermodynamic equilibrium in the sense that the function $(v, S) \mapsto \varepsilon(v, S)$ is strictly convex. It follows from (2.12) that

$$\begin{aligned}\varepsilon_v(v, S) &= -\frac{c_v(\gamma-1)T_*}{\rho_*^{\gamma-1}} v^{-\gamma} \exp\left(\frac{S - S_*}{c_v}\right) + p_\infty, \\ \varepsilon_S(v, S) &= T_* v_0^{\gamma-1} v^{1-\gamma} \exp\left(\frac{S - S_*}{c_v}\right).\end{aligned}$$

so that

$$\begin{aligned}\varepsilon_{vv}(v, S) &= \gamma\tfrac{c_v(\gamma-1)T_*}{\rho_*^{\gamma-1}} v^{-\gamma-1} \exp\left(\tfrac{S-S_*}{c_v}\right) > 0, \\ \varepsilon_{vS}(v, S) &= \tfrac{(\gamma-1)T_*}{\rho_*^{\gamma-1}} v^{-\gamma} \exp\left(\tfrac{S-S_*}{c_v}\right), \\ \varepsilon_{SS}(v, S) &= \tfrac{T_* v_0^{\gamma-1}}{c_v} v^{1-\gamma} \exp\left(\tfrac{S-S_*}{c_v}\right).\end{aligned} \tag{4.23}$$

A straightforward calculation shows that the determinant of the Hessian matrix of the function $(v, S) \mapsto \varepsilon(v, S)$ is given by

$$\varepsilon_{vv}\varepsilon_{SS} - \varepsilon_{vS}^2 = \frac{\frac{c_v(\gamma-1)T_*}{\rho_*^{\gamma-1}}}{c_v} T_* v_0^{\gamma-1} v^{-2\gamma} \exp\left(\frac{2(S - S_*)}{c_v}\right) > 0. \tag{4.24}$$

From (4.23) and (4.24) we deduce that the function $(v, S) \mapsto \varepsilon(v, S)$ is strictly convex. This is equivalent to that the function $(v, \varepsilon) \mapsto S(v, \varepsilon)$ is strictly concave, see Lem. 1.1, Chapter II, [17].

Our next argument is based on the following classical result. Assume that $\mathcal{U}$ is a strictly convex function in $\boldsymbol{R}^N$, and that there exists a function $\mathcal{F}$ and a vector-valued map f such that $D\mathcal{F} = D\mathcal{U}\, Df$. If U is a vector defined by

$$U = \frac{V+W}{2} + \frac{\theta}{2}(f(V) - f(W)),$$

then

$$\mathcal{U}(U) \leq \frac{\mathcal{U}(V) + \mathcal{U}(W)}{2} + \frac{\theta}{2}(\mathcal{F}(V) - \mathcal{F}(W)).$$

Let us choose

$$\mathcal{U}(U) = \rho g(S), \quad \mathcal{F}(U) = \rho u g(S), \tag{4.25}$$

where $g(S)$ is a strictly decreasing and convex function of S. First, we will show that $g(S)$ is a strictly convex function of $X = (v, \varepsilon)$. Indeed, the above result that S is strictly concave as a function of $X = (v, \varepsilon)$ means that for $0 < s < 1$ it holds

$$S(sX + (1-s)Y) > sS(X) + (1-s)S(Y)$$

for any X, Y. Now, the last inequality and that g is strictly decreasing and convex in S yield

$$\begin{aligned} g(S(sX + (1-s)Y)) &< g(sS(X) + (1-s)S(Y)) \\ &\leq sg(S(X)) + (1-s)g(S(Y)), \end{aligned}$$

for all X, Y, which demonstrate that $g(S)$ is a strictly convex function of $X = (v, \varepsilon)$. Therefore, the pair (4.25) is a convex entropy pair of the usual gas dynamics equations. The definition of the scheme (4.2) with the Lax-Friedrichs numerical flux yields

$$\mathcal{U}(U_j^{n+1}) \leq \frac{\mathcal{U}(U_{j-1,+}^n) + \mathcal{U}(U_{j+1,-}^n)}{2} + \frac{\theta}{2}(\mathcal{F}(U_{j-1,+}^n) - \mathcal{F}(U_{j+1,-}^n)),$$

for any entropy pair of the form (4.25). Thus, we have

$$\begin{aligned} \rho_j^{n+1} g(S_j^{n+1}) \leq \; & \tfrac{1}{2}\Big(\rho_{j-1,+}^n g(S_{j-1}^n) + \rho_{j+1,-}^n g(S_{j+1}^n)\Big) \\ & + \tfrac{\theta}{2}(\rho_{j-1,+}^n u_{j-1,+}^n g(S_{j-1}^n) - \rho_{j+1,-}^n u_{j+1,-}^n g(S_{j+1}^n)). \end{aligned}$$

Re-arranging terms, we obtain from the last inequality

$$\rho_j^{n+1} g(S_j^{n+1}) \leq \frac{1}{2}\rho_{j-1,+}^n (1 + \theta u_{j-1,+}^n) g(S_{j-1}^n) + \frac{1}{2}\rho_{j+1,-}^n (1 - \theta u_{j+1,-}^n) g(S_{j+1}^n).$$

It is easy to verify that the function $g(S) = (S_* - S)^p, p > 1$, where S_* is some constant such that $S_* - S > 0$, is strictly decreasing and convex for $S < S_*$. Applying the last inequality for $g(S) = (S_* - S)^p, p > 1$, we get

$$\begin{aligned} \rho_j^{n+1}(S_* - S_j^{n+1})^p \; & \leq \frac{1}{2}\rho_{j-1,+}^n (1 + \theta u_{j-1,+}^n)(S_* - S_{j-1}^n)^p \\ & + \frac{1}{2}\rho_{j+1,-}^n (1 - \theta u_{j+1,-}^n)(S_* - S_{j+1}^n)^p \\ & \leq \frac{1}{2}(\rho_{j-1,+}^n (1 + \theta u_{j-1,+}^n) \\ & + \frac{1}{2}\rho_{j+1,-}^n (1 - \theta u_{j+1,-}^n))\Big[\max\{S_* - S_{j-1}^n, S_* - S_{j+1}^n\}\Big]^p \\ & = \rho_j^{n+1}\Big[\max\{S_* - S_{j-1}^n, S_* - S_{j+1}^n\}\Big]^p, \end{aligned} \tag{4.26}$$

where the last equality follows from the definition of the scheme (4.2) with the Lax-Friedrichs numerical flux. Using the result of the part (i) that ρ_j^{n+1} is positive, canceling $\rho_j^{n+1} > 0$ on both sides of (4.26) we obtain

$$(S_* - S_j^{n+1})^p \leq \Big[\max\{S_* - S_{j-1}^n, S_* - S_{j+1}^n\}\Big]^p.$$

This gives

$$S_* - S_j^{n+1} \leq \max\{S_* - S_{j-1}^n, S_* - S_{j+1}^n\} = S_* - \min\{S_{j-1}^n, S_{j+1}^n\},$$

or

$$S_j^{n+1} \geq \min\{S_{j-1}^n, S_{j+1}^n\},$$

which establishes (4.18). The proof of Theorem 4.2 is complete. □

5. Numerical Tests

In this section we will present several numerical tests in which we compare the approximate solution and the exact Riemann solution. For simplicity, we assume that the fluid in each phase has the equation of state of a polytropic ideal gas. We take the parameters in the equations of state to be as follows:

$$\gamma_g = 1.4, \quad \gamma_s = 1.6, \quad c_{p,g} := \gamma_g c_{v,g} = 1.0087, \quad S_{g,*} = S_{s,*} = 0, \quad c_{p,s} := \gamma_s c_{v,s} = 4.1860. \tag{5.1}$$

The Lax-Friedrichs scheme is taken as the underlying scheme for (4.2) and (4.9). We also take

$$C.F.L = 0.5.$$

Exact solutions and approximate solutions of the Riemann problem for (1.1)-(1.2) with Riemann data

$$U(x,0) = \begin{cases} U_L, & x < 0, \\ U_R, & x > 0, \end{cases} \tag{5.2}$$

where U_L, U_R are constant states, will be computed and displayed on the interval $[-1, 1]$ of the x-space.

5.1. Test 1: A stationary wave

The approximate solution will be computed at the time $t = 0.01$ on the interval $[-1, 1]$ of the x-space with 500 mesh points. In this test, we consider the Riemann problem for (1.1)-(1.2) with the Riemann data (5.2) where U_L and U_R are given in Table 1.

Table 1

Components \ States	U_L	U_R
ρ_g	0.8	0.81355299
u_g	0.5	0.43704044
p_g	1	1.0237978
ρ_s	1	1.2850045
u_s	0	0
p_s	2	2.9872902
α_g	0.8	0.9

It is not difficult to check that in this case the Riemann solution results in the gas phase a stationary contact. Figure 1 shows that the stationary contact in the gas phase is well captured. It is easy to see that the contact wave belong to the subsonic region. However, the result still holds for data in the supersonic regions.

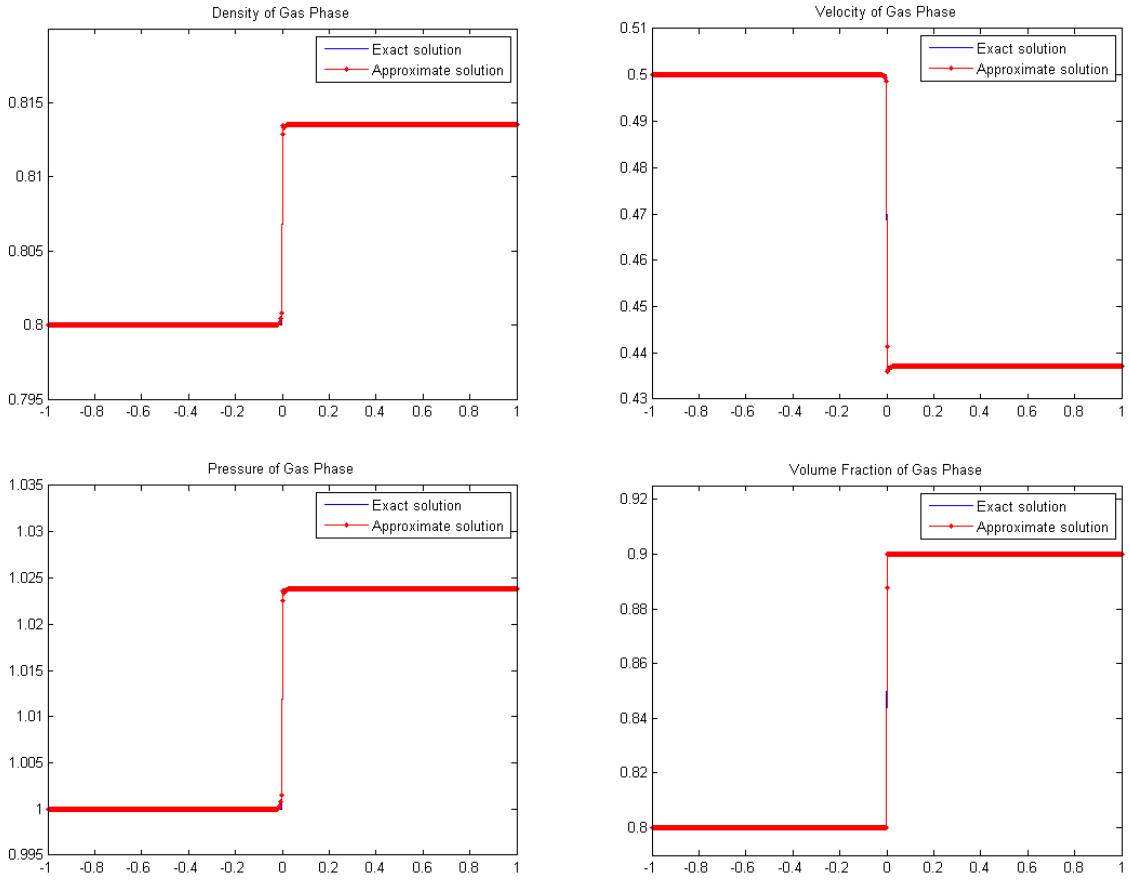

Figure 1: Test 1: The scheme (4.1)-(4.10) can capture equilibrium states in the gas phase

Recently, a numerical scheme designed for subsonic regions for more general model of two-phase flows has been constructed in [2]. This scheme also captures the above stationary contact wave in the gas phase, see Figure 2.

Thus, this test shows that our scheme as well the the scheme in [2]-designed for subsonic regions- are well-balanced in the gas phase in the sense that they can capture stationary contacts in the gas phase.

5.2. Test 2: Supersonic regions

In this test, the approximate solution will be computed at the time $t = 0.1$ on the interval $[-1, 1]$ of the x-space. We consider the Riemann problem for (1.1)-(1.2) with the Riemann data (5.2) where U_L and U_R are given in Table 2.

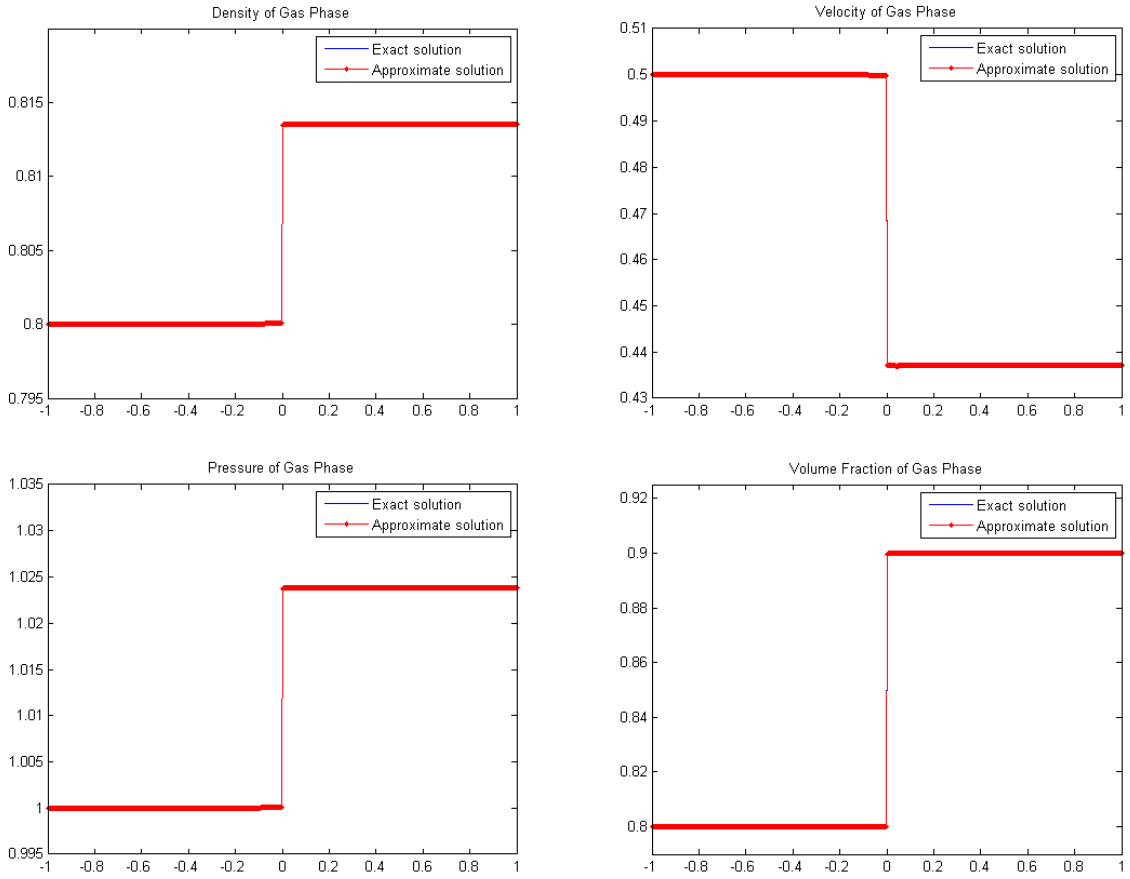

Figure 2: Test 1: The scheme in [2] can also capture equilibrium states in the gas phase

Table 2

Components\ States	U_L	U_R
ρ_g	0.08545023	0.17601423
u_g	-4.7689572	-5.1681691
p_g	0.3	0.83622836
ρ_s	0.93630573	1.1009669
u_s	0.21664237	0.20870557
p_s	1.8	2.3327532
α_g	0.5	0.55

One can easily verify that the Riemann data belong to the supersonic regions. The intermediate states that define the Riemann solution are given in Table 3.

Table 3				
$\diagdown$	U_1	U_2	U_3	U_4
ρ_g	0.13885662	0.2	0.2	0.17601423
u_g	-5.9309871	-5	-5	-5.1681691
p_g	0.6	1	1	0.83622836
ρ_s	0.93630573	0.93630573	1	1.0372987
u_s	0.21664237	0.21664237	0.1	0.1
p_s	1.8	1.8	2	2.1206848
α_g	0.5	0.5	0.5	0.55

The structure of the Riemann solution is described as follows. The Riemann solution first begins with a 1-shock wave from U_L to U_1, followed by a 3-rarefaction wave from U_1 to U_2, followed by a 4-shock wave from U_2 to U_3. The solution is then continued by a solid 5-contact from U_3 to U_4, and finally followed by a 3-rarefaction wave from U_4 to U_R. The exact Riemann solutions are drawn in Figures 3 and 4.

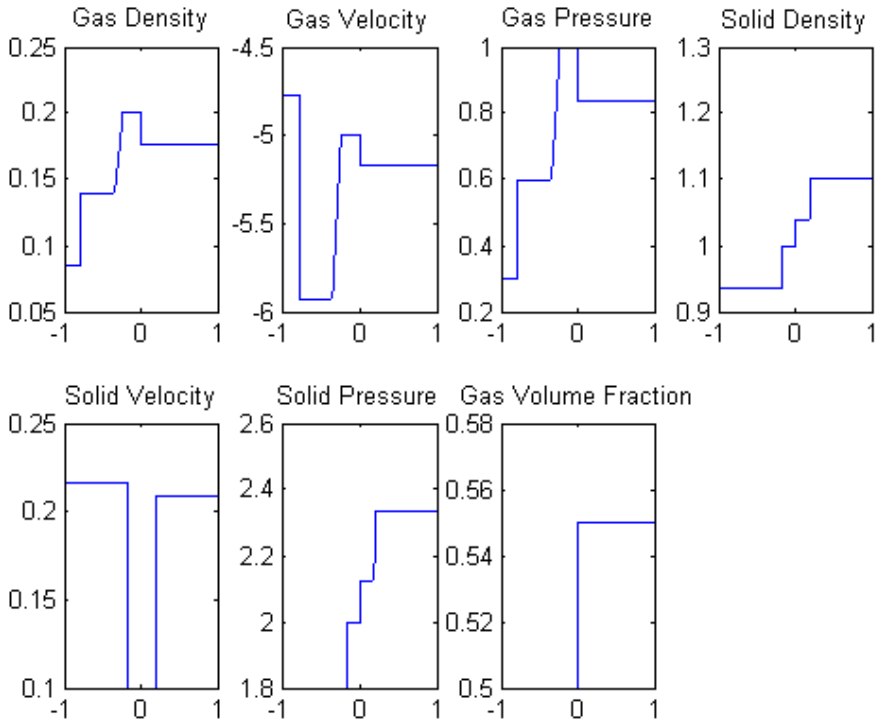

Figure 3: Test 2: Exact Riemann solution at the time $t = 0.1$

The errors for Test 2 are reported by the Table 4. Precisely, let us denote by $U_h = U_h(x,t)$ the approximate solution corresponding to the mesh-size h and by $U = U(x,t)$ the exact solution. In Table 4, we compute the values $||U_h(.,t=0.1) - U(.,t=0.1)||_{L^1(\boldsymbol{R})}$ and $||U_h(.,t=0.1) - U(.,t=0.1)||_{L^1} / ||U(.,t=0.1)||_{L^1}$, which represent the absolute error and the absolute relative error in the space $L^1(\boldsymbol{R})$, respectively, for different mesh-

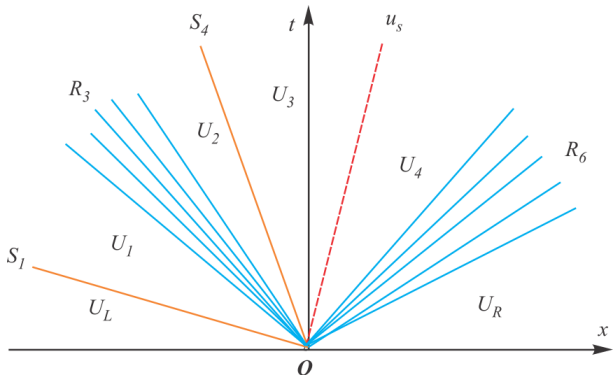

Figure 4: Test 2: Exact Riemann solution in the (x, t)-plane

sizes $h = \Delta x = 1/N$, where N takes the values $250, 500, 1000, 2000$ and 4000. Figures 5 and 6 show the exact and the approximate solutions with 500, 1000, and 4000 mesh points. One could see there is an additional wave in the solid velocity, which makes the configuration of the approximate solution different from the exact solution. *It seems that the scheme converges to a limit that slightly different from the exact solution in this case.* The scheme is numerically stable in the supersonic regions for this test.

Table 4

N	$\|\|U_h - U\|\|_{L^1}$	$\|\|U_h - U\|\|_{L^1}/\|\|U\|\|_{L^1}$	order
250	0.18519124	0.0092742091	–
500	0.12190857	0.0061050705	0.6
1000	0.078904635	0.0039514724	0.63
2000	0.052600668	0.0026341936	0.59
4000	0.036200786	0.0018129025	0.54

5.3. Test 3: Supersonic regions

In this test, the approximate solution will be computed at the time $t = 0.1$ on the interval $[-1, 1]$ of the x-space. We consider the Riemann problem for (1.1)-(1.2) with the Riemann data (5.2) where U_L and U_R are given in Table 5.

Table 5

Components\ States	U_L	U_R
ρ_g	0.3	0.49045078
u_g	5	4.9606427
p_g	0.2	0.39810826
ρ_s	1.1969795	1.2954081
u_s	-0.70474276	0.51451306
p_s	4	4.5391218
α_g	0.5	0.4

It is easy to check that the Riemann data belong to the supersonic regions, where many existing schemes may not work well. The intermediate states that define the Riemann solution are given in Table 6.

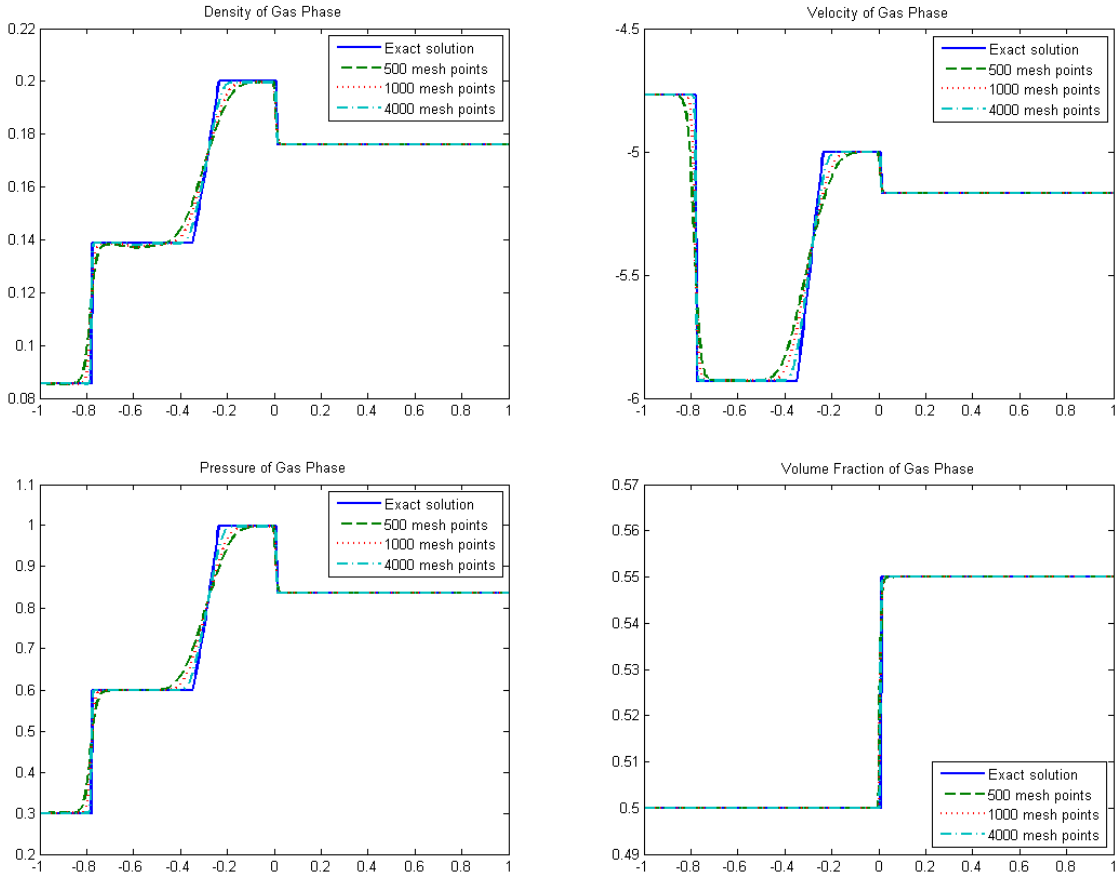

Figure 5: Test 2: The exact solution and approximate solution in the gas phase with different mesh-sizes

Table 6

$\diagdown$	U_1	U_2	U_3	U_4
ρ_g	0.3	0.37805592	0.37805592	0.43056368
u_g	5	4.9571588	4.9571588	4.8236071
p_g	0.2	0.27646407	0.27646407	0.33175688
ρ_s	1	0.9010034	1.2954081	1.2954081
u_s	-0.3	-0.3	0.51451306	0.51451306
p_s	3	2.5391218	4.5391218	4.5391218
α_g	0.5	0.4	0.4	0.4

The Riemann solution is a 4-rarefaction wave from U_L to U_1, followed by a 5-solid contact from U_1 to U_2, followed by a 6-rarefaction wave from U_2 to U_3, followed by a 1-shock wave from U_3 to U_4, and followed by a 3-rarefaction wave from U_4 to U_R. The exact solution are shown in Figures 7 and 8.

The errors for Test 3 are reported in the Table 7. We still denote by $U_h = U_h(x,t)$ the approximate solution corresponding to the mesh-size h and by $U = U(x,t)$ the exact solution. The values $||U_h(.,t=0.1) - U(.,t=0.1)||_{L^1(\boldsymbol{R})}$ and $||U_h(.,t=0.1) - U(.,t=$

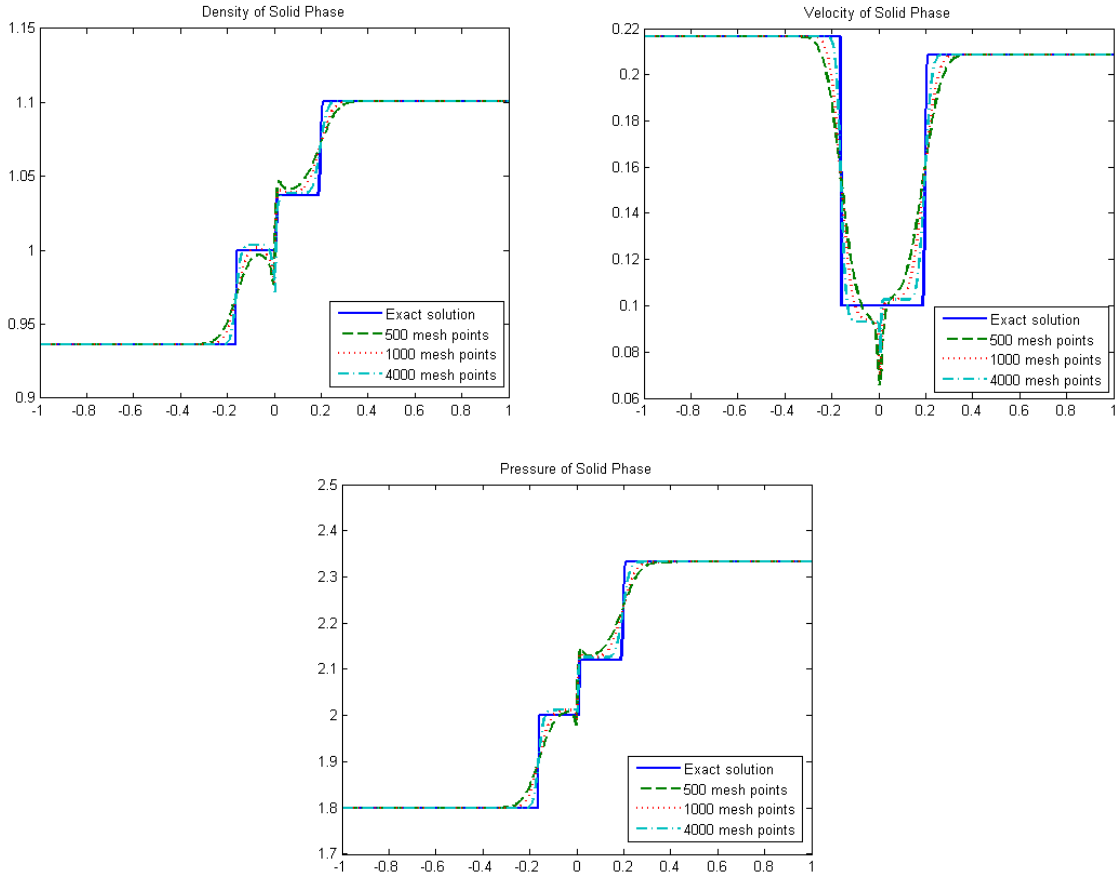

Figure 6: Test 2: The exact solution and approximate solution in the solid phase with different mesh-sizes

$0.1)||_{L^1}/||U(.,t=0.1)||_{L^1}$ are evaluated for different mesh-sizes $h = \Delta x = 1/N$, where N takes the values $250, 500, 1000, 2000$ and 4000. Figures 9 and 10 show the exact and the approximate solutions with 500, 1000, and 4000 mesh points. There is an additional wave in the quantities of the solid phase in Figure 10; *the approximate solutions seem to converge to a limit that slightly differ from the exact solution.* Again, the scheme is numerically stable in the supersonic regions for this test.

Table 7

N	$\|\|U_h - U\|\|_{L^1}$	$\|\|U_h - U\|\|_{L^1}/\|\|U\|\|_{L^1}$	order
250	0.27511093	0.011831599	–
500	0.19736281	0.0084879127	0.48
1000	0.14351663	0.0061721694	0.46
2000	0.10695992	0.0045999878	0.42
4000	0.082316009	0.0035401356	0.38

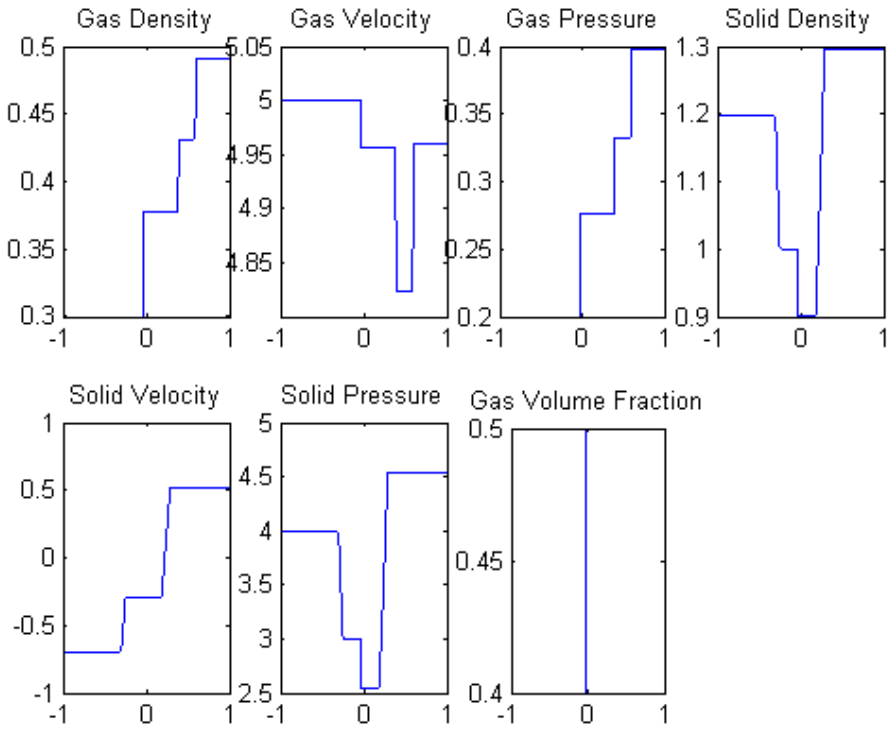

Figure 7: Test 3: Exact Riemann solution at the time $t = 0.1$

5.4. Test 4: Comparisons with other schemes in the subsonic region

In this test, we compare our method with various numerical methods in the literature with the well-tested case in [35]. The data are taken in the subsonic region, making the existing schemes, in particular schemes designed for subsonic regions, work well. Our scheme, however, seems to give a convergence to a function that visibly differs from the exact solution. Precisely, in this test $\gamma_g = \gamma_s = .4$, the approximate solutions are computed at the time $t = 0.2$ on the interval $[-1/2, 1/2]$, or $[0, 1]$. We consider the Riemann problem for (1.1)-(1.2) with the Riemann data (5.2) where U_L and U_R are given in Table 8.

Table 8

Components \ States	U_L	U_R
ρ_g	0.2	1
u_g	0	0
p_g	0.3	1
ρ_s	1	1
u_s	0	0
p_s	1	1
α_g	0.2	0.7

The exact Riemann solution were computed in [35]. Its intermediate states are given in Table 9.

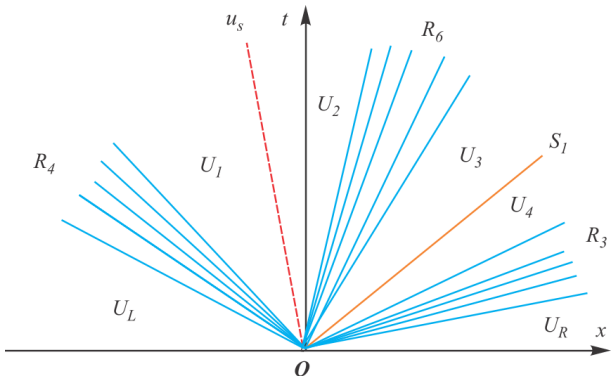

Figure 8: Test 3: Exact Riemann solution in the (x,t)-plane

Table 9

$\diagdown$	U_3	U_1	U_0	U_2	U_4
ρ_g	0.3266	0.3266	0.698	0.9058	1
u_g	-0.7683	-0.7683	-0.7683	-0.1159	0
p_g	0.6045	0.6045	0.6045	0.8707	1
ρ_s	1	0.9436	0.9436	1.0591	1.0591
u_s	0	0.0684	0.0684	0.0684	0.0684
p_s	1	0.9219	0.9219	1.0837	1.0837
α_g	0.2	0.2	0.2	0.7	0.7

The Riemann solution is a 1-shock wave from U_L to U_1, followed by a 4-rarefaction wave from U_L to U_3, followed by a 2-gas contact from U_1 to U_0, followed from a 5-solid contact from U_0 to U_2, followed by a 3-rarefaction wave from U_2 to U_4, followed by a 6-shock wave from U_4 to U_R. The configuration of the solution and the approximate solution by the scheme (4.1)-(4.10) with various mesh-sizes are shown in Figure 11.

The approximate solution by the scheme in [2] and is displayed in Figure 12 by courtesy of the authors. Comparisons between various schemes are given in [35] and are given in Figure 13, which was taken in [2].

In this test, we can see that the schemes in [2] and in [35] provide us with good approximations to the exact solution when the solution remain in the subsonic region. Our scheme gives approximate solutions that converge to a limit different from this exact solution. The difference between the exact solution and the approximate solution is quite large in the solid density and solid velocity. The result is better for the quantities in the gas phase.

6. Conclusions

The system (1.1)-(1.2) possesses complicated structures and cause standard numerical scheme to give unsatisfactory results. In this paper we build up a numerical method that consists of several procedures for the two-phase flow model (1.1)-(1.2). First we decompose the system into three subsystems of different performances. For each subsystem we apply a different numerical treatment. In the first subsystem consisting of the governing

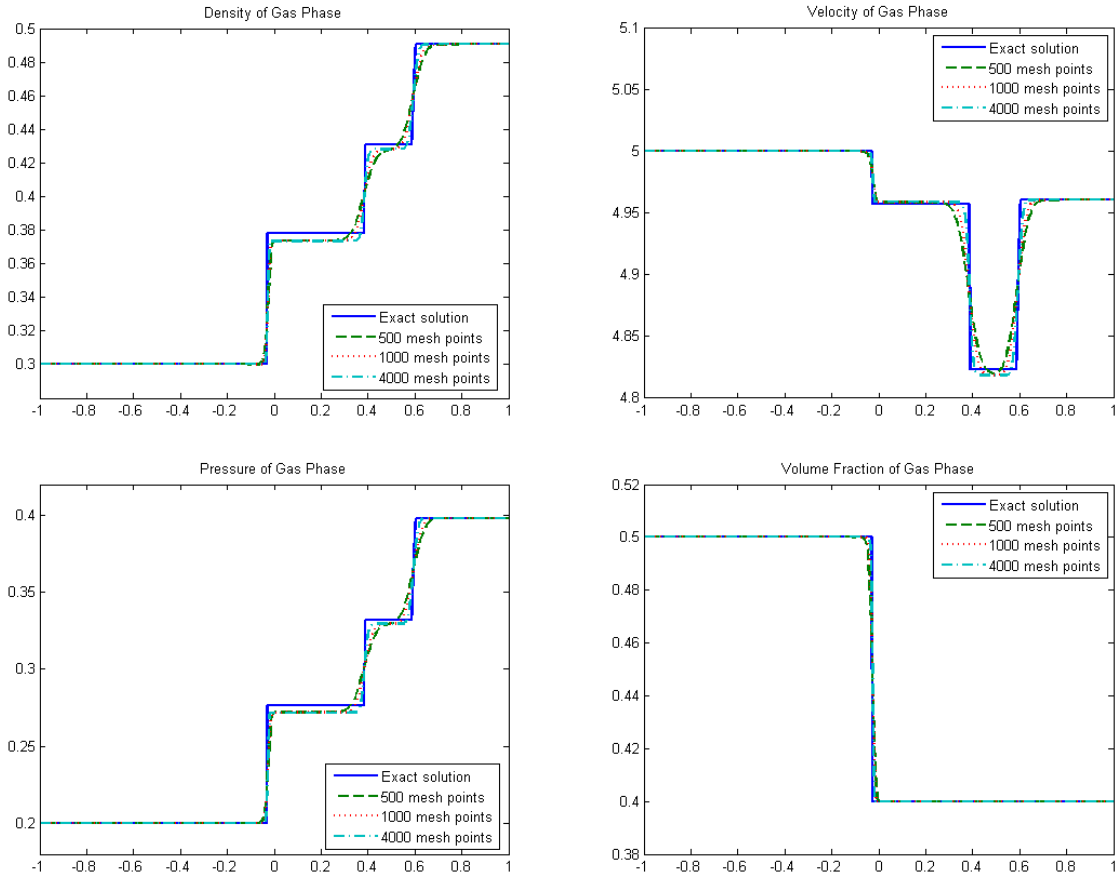

Figure 9: Test 3: The exact solution and approximate solution in the gas phase with different mesh-sizes

equations in the gas phase, we use stationary waves to absorb the nonconservative terms. In the second subsystem consisting of conservation laws of the mixture we can use a suitable scheme for conservation laws. In the third subsystem consisting of the compaction dynamics equation, we apply the technique of the Engquist-Osher scheme by observing that the solid velocity is constant across the solid contacts.

The scheme gives reasonably good results in the supersonic regions that are not always treated in existing schemes, but does not give satisfactory results in the subsonic region. However, it is robust, which is interesting. The results are better for the gas phase that absorbs the source term in the numerical scheme, which is not completely satisfactory. This suggests that the scheme could certainly be improved in that direction in order to get "similar" results for both phases.

The scheme is shown to possess some other nice properties: it can capture equilibrium states in the gas phase, it preserves the positivity of the volume fractions in both phases, it preserves the positivity of the density of the gas phase, and it satisfies the numerical minimum entropy principle in the gas phase.

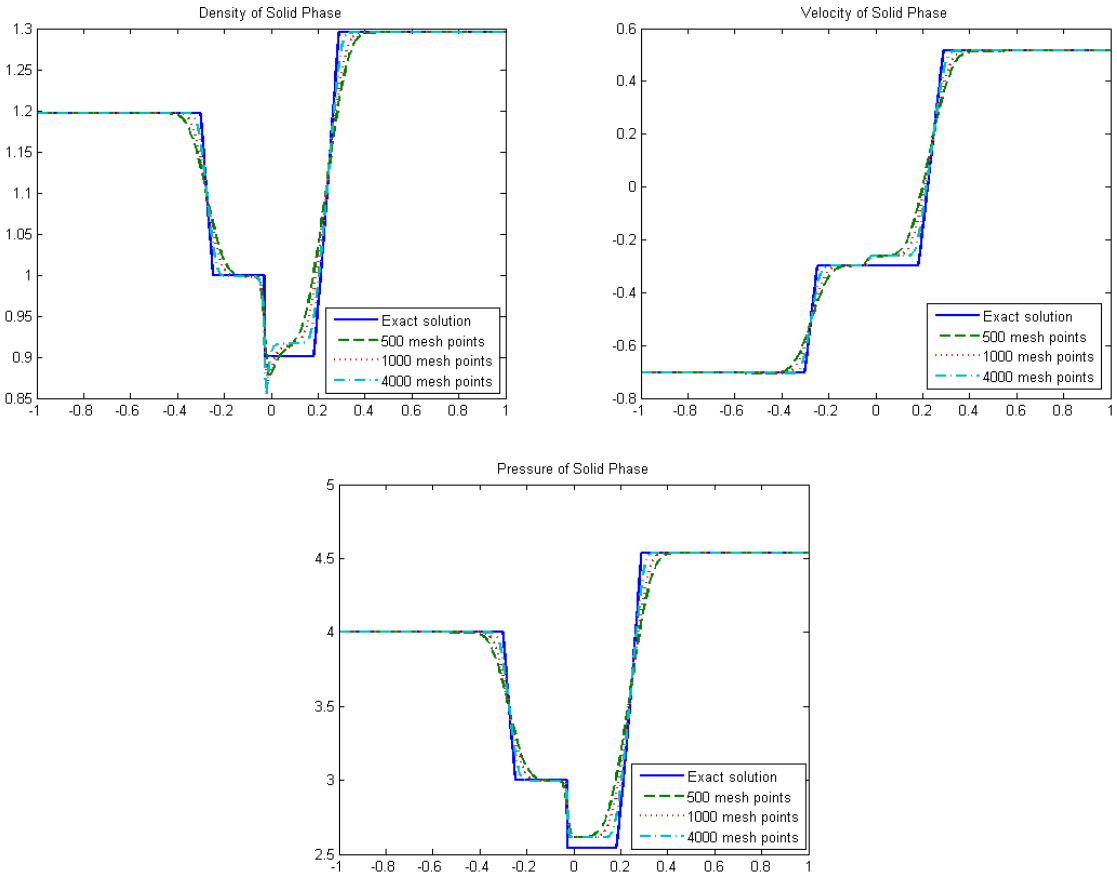

Figure 10: Test 3: The exact solution and approximate solution in the solid phase with different mesh-sizes

Acknowledgments

We would like to thank the reviewers for their very constructive and helpful comments and suggestions.

This research is funded by Vietnam National Foundation for Science and Technology Development (NAFOSTED) under grant number 101.02-2011.36.

References

[1] A. Ambroso, C. Chalons, F. Coquel, and T. Galié, Relaxation and numerical approximation of a two-fluid two-pressure diphasic model, *Math. Mod. Numer. Anal.*, 43 (2009), 1063-1097.

[2] A. Ambroso, C. Chalons, P.-A. Raviart, A Godunov-type method for the seven-equation model of compressible two-phase flow, *Computers & Fluids*, 54 (2012), 67-91.

[3] N. Andrianov, R. Saurel, G. Warnecke, A simple method for compressible multiphase mixtures and interfaces, Tech. Rep. 4247, INRIA (2001).

[4] N. Andrianov and G. Warnecke, The Riemann problem for the Baer-Nunziato model of two-phase flows, *J. Comput. Phys.*, 195 (2004), 434–464.

[5] E. Audusse, F. Bouchut, M-O. Bristeau, R. Klein, and B. Perthame, A fast and stable well-balanced scheme with hydrostatic reconstruction for shallow water flows, *SIAM J. Sci. Comput.*, 25 (2004), 2050–2065.

[6] M.R. Baer and J.W. Nunziato, A two-phase mixture theory for the deflagration-to-detonation transition (DDT) in reactive granular materials, *Int. J. Multi-phase Flow*, 12 (1986), 861–889.

[7] R. Bernetti, V.A. Titarev, and E.F. Toro, Exact solution of the Riemann problem for the shallow water equations with discontinuous bottom geometry. *J. Comput. Physic*, 227 (2008), 3212–3243.

[8] R. Botchorishvili, B. Perthame, and A. Vasseur, Equilibrium schemes for scalar conservation laws with stiff sources, *Math. Comput.*, 72 (2003), 131–157.

[9] R. Botchorishvili and O. Pironneau, Finite volume schemes with equilibrium type discretization of source terms for scalar conservation laws, *J. Comput. Phys.*, 187 (2003), 391–427.

[10] F. Bouchut, *Nonlinear stability of finite volume methods for hyperbolic conservation laws, and well-balanced schemes for sources*, Frontiers in Mathematics series, Birkhäuser, 2004.

[11] J.B. Bzil, R. Menikoff, S.F. Son, A.K. Kapila, and D.S. Steward, Two-phase modelling of a deflagration-to-detonation transition in granular materials: a critical examination of modelling issues, *Phys. Fluids*, 11(1999), 378–402.

[12] A. Chinnayya, A.-Y. LeRoux, and N. Seguin, A well-balanced numerical scheme for the approximation of the shallow water equations with topography: the resonance phenomenon. *Int. J. Finite Vol.*, 1(4), 2004.

[13] G. Dal Maso, P.G. LeFloch, and F. Murat, Definition and weak stability of nonconservative products, *J. Math. Pures Appl.*, 74 (1995), 483–548.

[14] T. Flåtten, A. Morin, and S.T. Munkejord, On solutions to equilibrium problems for systems of stiffened gases, *SIAM J. Appl. Math.*, 71 (2011), 41–67.

[15] T. Gallouët, J.-M. Hérard, and N. Seguin, Numerical modeling of two-phase flows using the two-fluid two-pressure approach, *Math. Models Methods Appl. Sci.*, 14 (2004), 663–700.

[16] P. Goatin and P.G. LeFloch, The Riemann problem for a class of resonant nonlinear systems of balance laws, *Ann. Inst. H. Poincar Anal. NonLinéaire*, 21 (2004), 881–902.

[17] E. Godlewski and P.-A. Raviart, *Numerical approximation of hyperbolic systems of conservation laws*, Springer-Verlag, New York, 1996.

[18] J.M. Greenberg and A.Y. Leroux, A well-balanced scheme for the numerical processing of source terms in hyperbolic equations, *SIAM J. Numer. Anal.*, 33 (1996), 1–16.

[19] J.M. Greenberg, A.Y. Leroux, R. Baraille, and A. Noussair, Analysis and approximation of conservation laws with source terms, *SIAM J. Numer. Anal.*, 34 (1997), 1980–2007.

[20] E. Isaacson and B. Temple, Nonlinear resonance in systems of conservation laws, *SIAM J. Appl. Math.*, 52 (1992), 1260–1278.

[21] E. Isaacson and B. Temple Convergence of the 2×2 godunov method for a general resonant nonlinear balance law, *SIAM J. Appl. Math.*, 55 (1995), 625–640.

[22] S. Jin and X. Wen, An efficient method for computing hyperbolic systems with gometrical source terms having concentrations, *J. Comput. Math.*, 22 (2004), 230–249.

[23] S. Karni and G. Hernández-Duenas, A Hybrid Algorithm for the Baer-Nunziato Model Using the Riemann Invariants, *J. Sci. Comput.*, 45 (2010), 382–403.

[24] D. Kröner, P.G. LeFloch, and M.D. Thanh, The minimum entropy principle for fluid flows in a nozzle with discntinuous crosssection, *Math. Mod. Numer. Anal.*, 42 (2008), 425–442.

[25] D. Kröner and M.D. Thanh, Numerical solutions to compressible flows in a nozzle with variable cross-section, *SIAM J. Numer. Anal.*, 43 (2005), 796–824.

[26] M-H. Lallemand and R. Saurel, Pressure relaxation procedures for multiphase compressible flows. *INRIA Report, No. 4038*, 2000.

[27] P.G. LeFloch, Shock waves for nonlinear hyperbolic systems in nonconservative form, *Institute for Math. and its Appl., Minneapolis, Preprint*, 593, 1989.

[28] P.G. LeFloch and M.D. Thanh, The Riemann problem for fluid flows in a nozzle with discontinuous cross-section, *Comm. Math. Sci.*, 1 (2003), 763–797.

[29] P.G. LeFloch and M.D. Thanh, The Riemann problem for shallow water equations with discontinuous topography, *Comm. Math. Sci.*, 5(2007), 865–885.

[30] R. Menikoff, Empirical equations of state for solids, *in Shock Wave Science and Technology Reference Library*, Volume 2 - Solids, Springer-Verlag, Berlin, 2007, pp. 143-188.

[31] R. Menikoff and B. Plohr, The riemann problem for fluid flow of real materials, *Rev. Modern Phys.*, 61 (1989), 75–130.

[32] S.T. Munkejord, Comparison of Roe-type methods for solving the two-fluid model with and without pressure relaxation, *Computers & Fluids*, 36 (2007), 1061–1080.

[33] G. Rosatti and L. Begnudelli, The Riemann Problem for the one-dimensional, free-surface Shallow Water Equations with a bed step: theoretical analysis and numerical simulations, *J. Comput. Phys.*, 229 (2010), 760–787.

[34] R. Saurel and R. Abgrall, A multi-phase Godunov method for compressible multifluid and multiphase flows, *J. Comput. Phys.*, 150 (1999), 425–467.

[35] D.W. Schwendeman, C.W. Wahle, and A.K. Kapila, The Riemann problem and a high-resolution Godunov method for a model of compressible two-phase flow, *J. Comput. Phys.*, 212 (2006), 490–526.

[36] M.D. Thanh, On a two-fluid model of two-phase compressible flows and its numerical approximation, *Commun. Nonlinear Sci. Numer. Simulat.*, 17 (2012), 195-211.

[37] M.D. Thanh, The Riemann problem for a non-isentropic fluid in a nozzle with discontinuous cross-sectional area, *SIAM J. Appl. Math.*, 69 (2009), 1501–1519.

[38] M.D. Thanh, Md. Fazlul K., and A.I. Md. Ismail, Well-balanced scheme for shallow water equations with arbitrary topography, *Inter. J. Dyn. Sys. and Diff. Eqs.*, 1(2008), 196–204.

[39] M.D. Thanh and A.I. Md. Ismail, Well-balanced scheme for a one-pressure model of two-phase flows, *Phys. Scr.*, 79 (2009), 065401 (7pp).

[40] M.D. Thanh, D. Kröner, and N.T. Nam, Numerical approximation for a Baer-Nunziato model of two-phase flows, *Appl. Numer. Math.*, 61 (2011), 702–721.

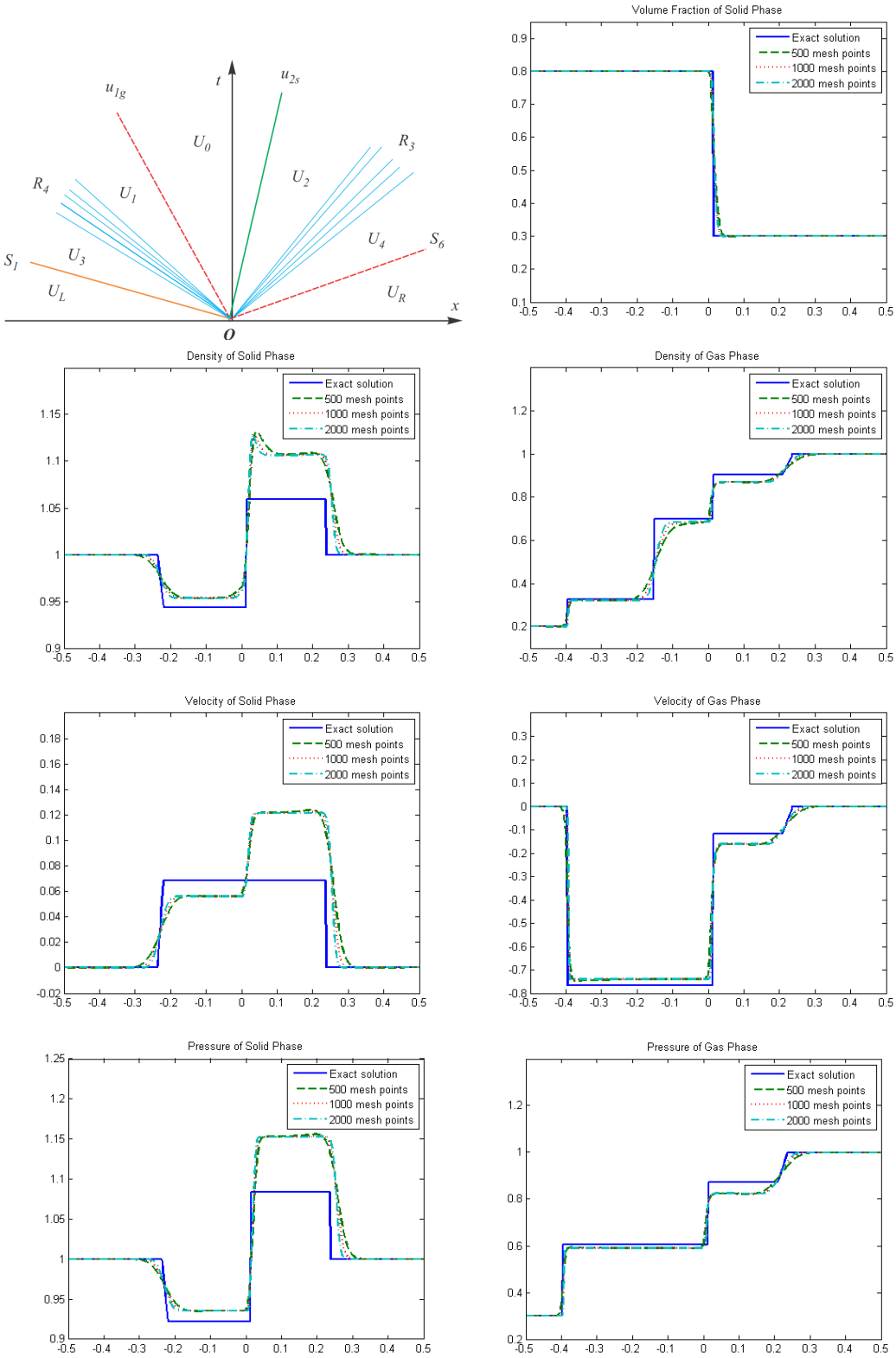

Figure 11: Test 4: The exact solution (upper-left corner) and approximate solution with different mesh-sizes by the scheme (4.1)-(4.10)

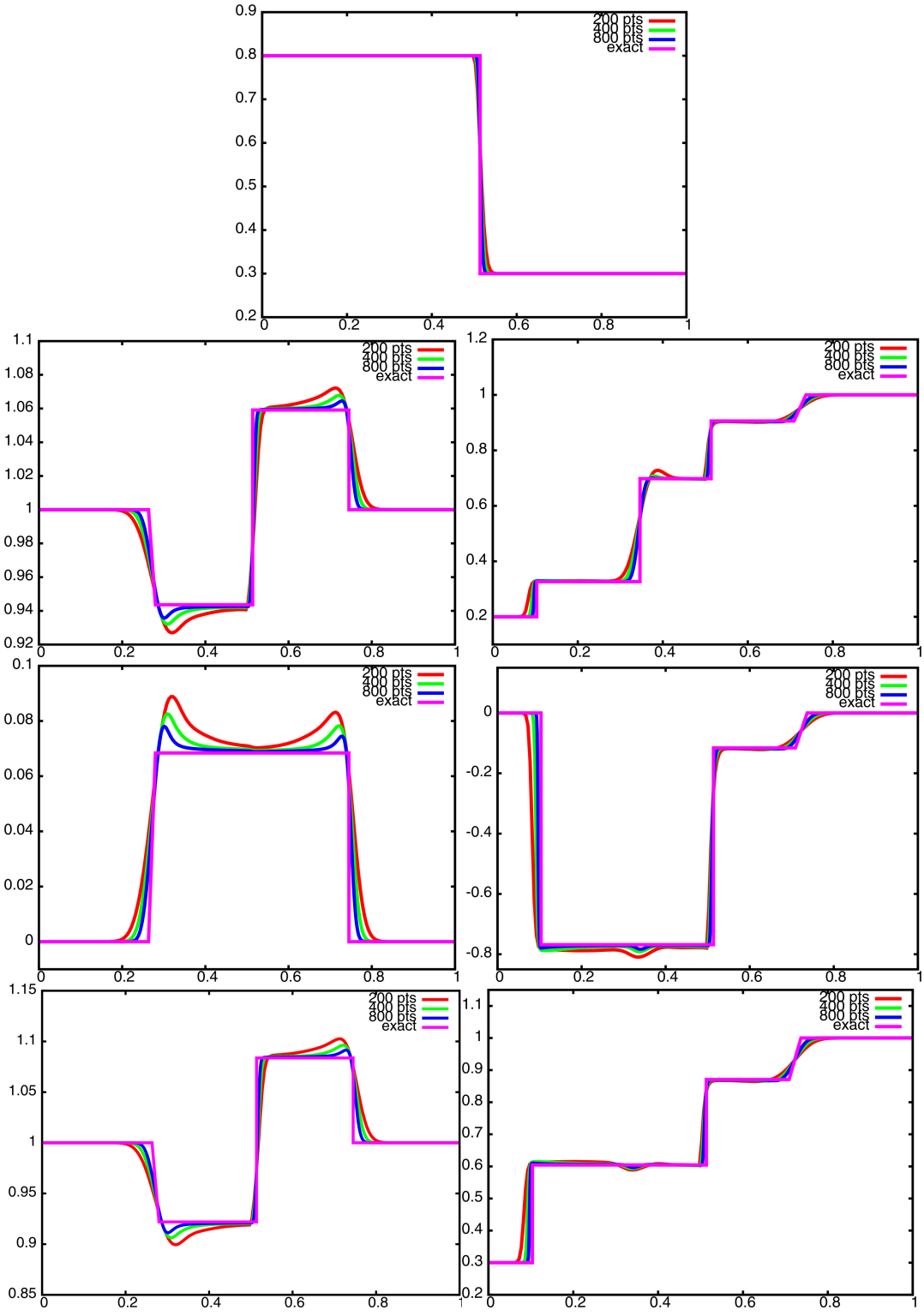

Figure 12: Test 4: The approximate solution by the scheme in [2] by courtesy of the authors.

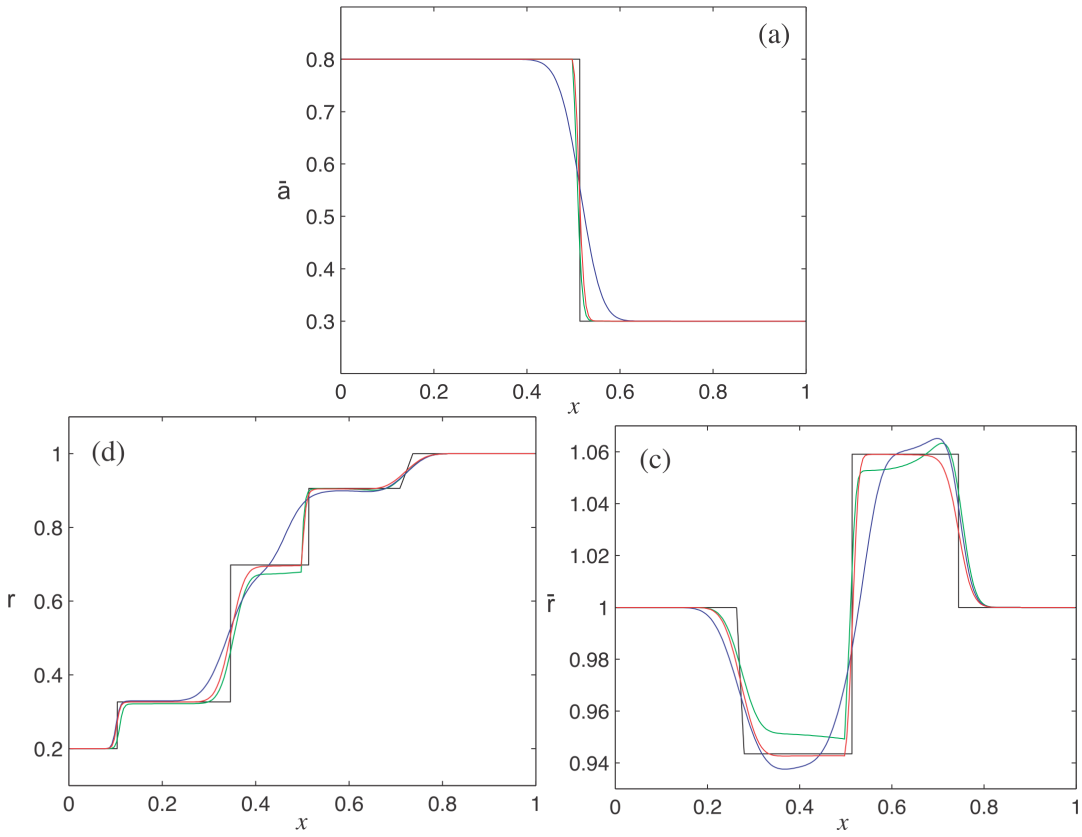

Figure 13: Test 4: The approximate solution by various schemes given in [35]. These pictures were taken from [2]. The approximate solution by blue curve is given by the method in [34]; the approximate solution by green curve is given by the method in [3], the approximate solution by red curve is given by the method in [35], all with 200 grid cells. The exact solution appears in black.